Kinome-wide synthetic lethal screen identifies PANK4 as modulator of resistance in glioblastoma

Viviana Vella
University of Sussex
Angeliki Ditsiou
University of Sussex
Anna Chalari
Biomedical Research Foundation of the Academy of Athens
Murat Eravci
University of Sussex
Sarah K Wooler
University of Sussex
Teresa Gagliano
University of Udine
Cecilia Bani
University of Sussex
Emanuela Kerschbamer
University of Udine
Frances M.G. Pearl
University of Sussex
Gianluca Lopez
University of Milan
Ling Peng
Xinqiao Hospital, Army Medical University
Justin Stebbing
Anglia Ruskin University
Apostolos Klinakis
Biomedical Research Foundation of the Academy of Athens
Georgios Giamas (g.giamas@sussex.ac.uk)
University of Sussex
Bin Xu
Renmin Hospital of Wuhan University
Yongchang Zhang
Hunan Cancer Hospital/The Affiliated Cancer Hospital of Xiangya School of Medicine

Research Article

Keywords: GBM, TMZ resistance, Synthetic lethality, Kinome-wide RNAi screen, Kinases, Pseudokinases, PANK4, DUF89 domain, TMT-based quantitative proteomics, Cellular detoxification

Posted Date: March 27th, 2023

DOI: https://doi.org/10.21203/rs.3.rs-2731966/v1

Additional Declarations: No competing interests reported.

Version of Record: A version of this preprint was published at Advanced Science on February 14th, 2024. See the published version at https://doi.org/10.1002/advs.202306027.

Abstract

Temozolomide (TMZ) represents the cornerstone of therapy for glioblastoma (GBM). However, acquisition of resistance limits its therapeutic potential and therefore poses the need to identify new therapeutic combinations that could improve treatment outcomes. Despite the human kinome has proved to be an undisputable source of druggable targets, our knowledge remains confined to a limited fraction of it, with a multitude of under-investigated proteins yet to be characterised. Using a kinome-wide RNAi screen, we found that abrogation of pantothenate kinase 4 (PANK4) enhances the antiproliferative effects of TMZ in GBM *in vitro*. Further validation of our top-hit across various TMZ-resistant GBM cell models, patient-derived GBM cell lines and tissue samples, as well as *in vivo* studies, corroborated the potential translational significance of our findings. We showed that PANK4 expression is induced during TMZ treatment, and its expression is associated with a worse clinical outcome. Using a Tandem Mass Tag (TMT)-based quantitative proteomic approach, a comprehensive global protein dynamics analysis was undertaken to identify key response signatures upon PANK4 knockdown, in the presence or absence of TMZ. We revealed that silencing of PANK4 leads to a marked downregulation of a subset of proteins involved in cellular detoxification. More specifically, as cells undergo genotoxic stress during TMZ exposure, PANK4 depletion represents a synthetic vulnerability, focal point that can lead to critical cellular damage, accumulation of toxic metabolites, and subsequent cell death. Taken together, we unveil a previously unreported role for PANK4 in mediating therapeutic resistance to TMZ in GBM.

Introduction

Glioblastoma multiforme (GBM) is one of the most aggressive and lethal forms of primary brain and central nervous system (CNS) tumours, and it is essentially an incurable disease (1–3). The current mainstay of treatment for GBM patients is multimodal, as it consists of maximal surgical resection, followed by localized radiotherapy (RT) combined with concomitant and adjuvant chemotherapy with the alkylating agent temozolomide (TMZ) (1). Acquisition of resistance to TMZ, is one of the main reasons why chemotherapy generally fails, posing a great challenge for the management of GBM patients (3).

As in the case of other cancers (4, 5), aberrations in diverse core kinase-signalling pathways have proved to be crucial for GBM initiation and progression and hence they have been intensively investigated (6, 7). Nevertheless, the human kinome encompasses a multitude of under-investigated kinases with potential therapeutic relevance that may represent viable drug targets (8–10), albeit their role still remains unexplored in GBM therapeutic resistance. Intriguingly, pseudokinases represent a notable, yet poorly understood, fraction of the kinome, which has garnered increased interest over the last few years (11–13). By signalling primarily through noncatalytic mechanisms, along with their unique structural features, pseudokinases play a critical role both in normal physiology and pathological conditions, including cancer (11–15).

Pantothenate kinase 4 (PANK4) is an understudied but highly conserved protein (16). Unlike the other three members of the pantothenate kinases family (PANK1-3), PANK4 has been characterised as a

pseudokinase, due to mutations of specific residues that have rendered its kinase domain catalytically inactive (16). Interestingly, PANK4 also encompasses a C-terminal phosphatase domain (DUF89) implicated in metabolite damage-control processes (17). The limited number of existing studies have mainly attempted to examine its catalytic activity as well as its metabolic role in the biosynthesis of coenzyme A (CoA) and in the context of pantothenate kinase–associated neurodegeneration (PKAN) disorders (16–19). Still, to date, its functional spectrum in physiological processes, cancer and other diseases, remains to be determined.

In this study, through a kinome-wide RNAi screen, we identified PANK4 as a synthetic lethal partner of TMZ in drug-resistant GBM cells and demonstrated that its depletion enhances the effect of TMZ, improving the response to TMZ therapy. More specifically, we showed that combined abrogation of PANK4 and TMZ treatment leads to attenuation of cell proliferation and clonogenicity, increased cell death in TMZ-resistant GBM models, as well as decreased tumour growth *in vivo*. We also provide evidence that PANK4 expression is induced in response to TMZ treatment and increased PANK4 levels are associated with a worse clinical outcome. Moreover, by employing TMT-based quantitative proteomics, we reveal a link between PANK4 and a set of proteins of the cellular detoxification system, consistent with its role in damage control (17, 20). Our findings illustrate that PANK4 depletion exacerbates the damage caused by TMZ by compromising the cellular detoxification mechanisms and shifting the balance towards an inefficient stress response, ultimately leading to cell death. In aggregate, we investigate the uncharacterised, yet highly attractive role of PANK4 in the context of TMZ resistance in GBM.

Results

Kinome-wide RNAi screen identifies PANK4 as a synthetic lethal partner of TMZ

To explore the role of protein kinase signalling in TMZ resistance, we established the experimental pipeline shown in Fig. 1A. A kinome-wide RNAi screen using a small interfering RNA (siRNA) library was performed. Briefly, TMZ-resistant U87MG cells derived from the “Resistant Cancer Cell Line (RCCL) collection” and generated by chronic exposure to the drug (from now on referred to as $U87MG^{Res}$) (21), were transfected with siRNA pools targeting each of the 709 human protein kinase and kinase-related genes *(Day 1)* and treated with a sublethal dose of TMZ or DMSO *(Day 2)*. Subsequently, differences in cell proliferation following siRNA knockdown and TMZ treatment were assessed *(Day 6)*.

The primary screen was performed twice and the biological reproducibility of the two screen experiments was evaluated showing good statistical correlation (**Supplementary Fig. 1A**). As the purpose of this study was to identify drug/siRNA combinations that resulted in a synthetic lethal effect, a sublethal concentration of TMZ able to inhibit cell proliferation by 20% (IC_{20}) was used for this screen (**Supplementary Fig. 1B**). Similarly, as for the data generated from the primary screens (**Supplementary Table S1**), all gene candidates having an independent effect of > 20% on cell proliferation were excluded

from further analysis. This way, we sought out to uncover targets that are critical for cell proliferation only in the presence of the drug, and therefore display a synthetic lethal effect with TMZ. Under these conditions, we unveiled 22 statistically significant top-ranking genes as potential targets in our GBM cell model, with PANK4 being the most effective hit (Fig. 1B and **Supplementary Fig. 1C**).

To further assess the biological reproducibility of our results, we implemented a secondary screen on the same TMZ-resistant GBM cell model. A number of randomly selected kinases was used for confirmation. Consistent effects were observed across the independent screens, proving the ability of the selected kinases to reproduce the synthetic lethal phenotype observed in our primary screens (Fig. 1C).

Taken together, based on its highest z-score rank and considering its largely unexplored, yet intriguing role in cancer, we focused on PANK4 in order to investigate its potential role as chemosensitizer of TMZ in GBM.

PANK4 knockdown enhances the chemosensitivity of TMZ-resistant GBM cells

The prospect of PANK4 as a target for re-sensitisation to TMZ treatment was assessed across additional TMZ-resistant GBM cells (21, 22). These included drug-resistant T98G and U251 cells (from now on referred to as $T98G^{Res}$ and $U251^{Res}$ respectively) that were established following continuous exposure of their parental counterparts to increasing TMZ concentrations (21, 22), as well as the inherently TMZ-resistant T98G cell line (from now on referred to as $T98G^{Par}$).

Variable PANK4 protein expression levels and different drug susceptibility profiles were observed across the tested cell lines, therefore a sublethal concentration of TMZ able to inhibit cell proliferation by 20% was determined for each cell line (IC_{20}) (Fig. 2A). All our drug-resistant cell models were then assessed under the same conditions used in the original screen (Fig. 1A). Combined PANK4 silencing and treatment with sublethal doses of TMZ were able to potentiate the effect of TMZ in a synergistic manner, leading to a decrease in cell proliferation (Figs. 2B and 2C). Moreover, a significant impairment of cell proliferation was observed upon silencing of PANK4 and treatment with increasing concentrations of TMZ (Fig. 2D). Similar antiproliferative effects were also detected in patient-derived GBM cell lines obtained from the “Human Glioblastoma Cell Culture” (HGCC) biobank (23), where knockdown of PANK4 followed by TMZ treatment led to an improved response to the drug (Fig. 2E).

To corroborate our findings, we next assessed whether the observed phenotype could be rescued through gain-of-function experiments in stably PANK4-depleted $T98G^{Res}$ cells. As shown in Fig. 2F, re-expression of PANK4 abrogated sensitivity to TMZ treatment, restoring resistance to the drug. All PANK4-targeting RNAi tools were validated for their ability to provide efficient and sustained PANK4 knockdown as shown in **Supplementary Fig. 2** (**A-E**).

Altogether, our results support that combined silencing of PANK4 and TMZ treatment synergistically impede proliferation of drug-resistant GBM cells, further emphasising the chemo-sensitising potential of

PANK4 depletion.

PANK4 depletion potentiates TMZ cytotoxicity by reducing the clonogenic potential of resistant GBM cell lines

To test whether silencing of PANK4 also has a long-term chemo-sensitising effect in our resistant GBM cell models following exposure to TMZ, we conducted clonogenic cell survival assays. Our results showed that the colony-forming ability of $T98G^{Res}$ and $U87MG^{Res}$ cells treated with TMZ was significantly impaired following silencing of PANK4 (Figs. 3A and 3B). The observed decrease in clonogenicity further supports our notion that PANK4 depletion enhances TMZ cytotoxicity, rendering TMZ-resistant GBM cells more susceptible to the treatment.

PANK4 downregulation induces apoptotic cell death upon TMZ treatment

The phenotype resulting from simultaneous PANK4 knockdown and TMZ treatment was contradistinguished by a significant decrease in cell proliferation and induction of cell death. To examine this effect, we measured the apoptosis levels using annexin V and 7-AAD (7-aminoactinomycin D) staining. Neither treatment with sublethal concentrations of TMZ or silencing of PANK4 alone were able to significantly affect cell viability or induce apoptosis. However, a pronounced reduction in cell viability and a robust increase in the percentage of apoptotic cells was observed following combined PANK4 depletion and TMZ treatment (Figs. 4A and 4B). Moreover, assessment of a set of apoptotic markers confirmed that TMZ treatment combined with PANK4 knockdown trigger the activation of apoptotic signalling pathways, by downregulating MCL1 (myeloid cell leukemia-1) (24) and activating caspase 3 (25) (Fig. 4C). A schematic representation of the process is shown in Fig. 4D. In summary, PANK4 silencing enhances cell death by activating apoptotic signalling pathways following TMZ treatment.

Abrogation of PANK4 sensitises chemo-resistant GBM tumours to TMZ treatment in vivo

Our aforementioned cell-based assays demonstrated that while silencing of PANK4 displays modest phenotypic effects, PANK4 knockdown in combination with TMZ treatment significantly potentiates TMZ cytotoxicity, sensitising TMZ-resistant GBM cells to the drug. To validate our findings *in vivo*, we established the experimental pipeline summarised in Fig. 5A. Firstly, we assessed the effect of PANK4 silencing and confirmed its effective knockdown. Consistent with our *in vitro* results, no significant changes were observed on tumour growth in the absence of the drug (Fig. 5B). Following establishment of a sublethal TMZ concentration (IC_{20}) *in vivo* (Figs. 5C and 5D), we evaluated the effect of TMZ treatment either alone or in combination with PANK4 knockdown. While treatment of mice with sublethal doses of TMZ did not significantly affect tumour growth, susceptibility to the drug was significantly improved following PANK4 silencing, as shown by the pronounced reduction in tumour growth (Figs. 5E and 5F, **Supplementary Table S2**). Moreover, in support of our *in vitro* results, immunohistochemical (IHC) analysis showed no significant changes in Ki-67 expression upon PANK4 silencing or TMZ treatment

alone (Figs. 5G and 5H). However, a considerable decrease in proliferation was detected in harvested tumours following PANK4 depletion and TMZ treatment (Fig. 5H).

In line with our *in vitro* findings, PANK4 depletion positively modulates sensitivity to TMZ *in vivo* and renders chemo-resistant tumours more vulnerable to the drug, further highlighting PANK4 as a synthetic lethal partner of TMZ.

PANK4 expression profile in GBM patient cohorts and its association with TMZ resistance

To evaluate the clinical relevance of PANK4 expression in GBM tumours, we analysed the REMBRANDT (Repository of Molecular Brain Neoplasia Data) dataset (26). No significant differences in PANK4 mRNA levels were observed between GBM tumours and normal brain tissue (Fig. 6A). Nevertheless, in line with previous studies on acute myeloid leukemia (AML) (27), Kaplan-Meier survival analysis revealed that increased PANK4 mRNA expression is associated with decreased overall survival (OS) of patients suffering from GBM (Fig. 6B). In agreement with these data, our immunohistochemical (IHC) analysis performed on a cohort of GBM patients further suggested a link between reduced PANK4 expression levels and improved OS (Fig. 6C and **Supplementary Fig. 3A**).

To further explore the association between PANK4 expression and TMZ resistance, we used the Gene Expression Omnibus database (GEO; accession number: GSE68029) and examined kinases that were previously reported to be differentially expressed in TMZ-resistant and parental GBM stem cells (GSCs) (28, 29). Intriguingly, PANK4 was found to be upregulated in the TMZ-resistant group compared with parental cells that were sensitive to the drug. (Fig. 6D). Further analysis of the TMZ-resistant group revealed significantly higher PANK4 mRNA levels in TMZ-resistant GSCs that survived two cycles of TMZ treatment over GSCs that survived one cycle of TMZ treatment only (Fig. 6E) (28).

Therefore, we next sought to determine whether PANK4 expression may be induced during TMZ treatment. To/assess this, U87MG and T98G parental cells (referred to as $U87MG^{Par}$ and $T98G^{Par}$ respectively) were treated with TMZ for different time points. Treatment with the drug triggered a progressive increase both in PANK4 mRNA (**Supplementary Figs. 3B and 3C**) and protein expression levels (Figs. 6F and 6G). In addition, our TMZ-resistant cell lines displayed notably higher PANK4 protein levels than their parental counterparts (Fig. 6H).

Combined, these findings support that PANK4 expression is prompted in response to TMZ treatment and elevated PANK4 levels are maintained in cells that have acquired a resistant phenotype (Fig. 6I). This suggests that PANK4 expression could be induced during TMZ chemotherapy, implying a potential requirement for PANK4 in response to TMZ.

TMT-based proteomic analysis reveals reduced cell detoxification response upon PANK4 knockdown

To further explore the contribution of PANK4 to TMZ resistance, we performed a comprehensive proteomic characterisation of TMZ-resistant GBM cells using a quantitative Tandem Mass Tagging (TMT)-based proteomic approach (**Supplementary Table S3**), as summarised in Fig. 7A. It has recently been shown that PANK4 is a pseudokinase harbouring substitutions of two key residues in the catalytic domain (Glu138Val and Arg207Trp), which are required for its kinase activity (16). Notably, PANK4 is characterised by a DUF89 phosphatase domain that has been reported to possess damage-control functions (Fig. 7B) (17). By participating to the so-called damage pre-emption processes (also named 'housecleaning' processes), the DUF89 domain is held accountable for the removal of potentially harmful build-ups of metabolites or side products (17, 20).

Given the largely unexplored functions of PANK4, we initially focused on changes in protein abundance following PANK4 silencing. Global proteomic analysis resulted in the identification of 6,756 peptides of which 1,005 were significantly altered after PANK4 knockdown ($p < 0.05$) (Fig. 7C and **Supplementary Fig. 4A**). Interestingly, Gene Ontology (GO) over-representation analysis of statistically significant deregulated proteins, uncovered a marked downregulation of biological processes (BP) linked to "cellular detoxification", "cellular response to toxic substance" and "detoxification"; these being among the top 20 downregulated biological processes impacted by PANK4 depletion (Fig. 7D). Dissection of the above-mentioned downregulated processes unveiled a host of proteins (GSTP1, NQO1, PRDX3, PRDX1, ADH5, SRXN1, DHFR, GSTM2, ESD, ALDH1A1, GSTM3, MTARC2, AKR1B10, PARK7) with central roles in cellular protection against various types of harmful metabolites (Figs. 7E and 7F) (30–38). Importantly, numerous toxic metabolites can accumulate within the cell and, if not adequately cleared, lead to detrimental consequences, emphasising the importance for cells to rely on efficient detoxification systems (39). Of note, a few of the proteins we identified (including PARK7, PRDX1, NQO1, GSTP1, PRDX3, GSTM3, ALDH1A1, SRXN1 and GSTM2) are linked to cellular protection against oxidative stress in GBM (30–36), and other cancers (37, 38, 40–42), suggesting that PANK4 may take part to the cellular detoxification response by preventing stress overload, including damage due to oxidative stress (Fig. 7G). Moreover, enrichment analysis of significantly downregulated proteins, in PANK4-depleted cells treated with TMZ (Fig. 7H and 7I), revealed that "cellular response to oxidative stress" was one of the top 20 significantly downregulated biological processes, resulting in deregulation of a subset of proteins, as shown in Fig. 7J.

To further support our observations, we also ran Gene Set Enrichment Analysis (GSEA) on all PANK4-modulated proteins and found a significant downregulation of the GO "cellular response to oxidative stress" process upon PANK4 knockdown, both alone and in combination with TMZ (**Supplementary Fig. 4B and 4C**, respectively). Similar results were also obtained following TMZ treatment (**Supplementary Fig. 4D**). Consistent with our proteomic data, determination of intracellular ROS levels in TMZ-resistant GBM cells showed a surge in ROS levels especially following combined PANK4 silencing and TMZ treatment (**Supplementary Fig. 4E**).

Taken together, our data suggest a novel protective role for PANK4 in the context of TMZ-resistant GBM cells. Importantly, loss of PANK4 can tip the balance towards an impaired detoxification response and

subsequently lead to damage accumulation and cell death.

Discussion

Resistance to TMZ remains a major challenge in the treatment of GBM, with most patients developing recurrence, and displaying a poor survival rate (1–3). While several hallmarks of chemo-resistance in GBM have been described and intensively studied (43–46), there are still some poorly explored areas of research, holding great therapeutic potential, that are worthy of investigation. The interest in kinases and pseudokinases has considerably grown over the past years owing to their versatile nature (11–14). In particular for pseudokinases, despite being regarded as 'inert' due to their defective catalytic activity, their active role in physiology and disease, as well as in drug-resistance (47–49), has put them at the centre of an ever-growing and dynamic area of research.

Our study provides evidence supporting a previously unreported role for PANK4 in mediating resistance to TMZ chemotherapy in GBM. Our *in vitro* data demonstrate that concomitant PANK4 abrogation and TMZ treatment can reverse chemo-resistance by reducing cell proliferation, colony formation potential and increasing cell apoptosis on a number of TMZ-resistant GBM cell models, while sensitising GBM tumours to TMZ treatment *in vivo*. These results add to our understanding of PANK4 function, an overlooked member of the pantothenate kinase family carrying a kinase domain that has undergone inactivation due to evolutionary mutations (16, 17). Because of its lack of catalytic activity, PANK4 has largely been neglected. The limited number of available studies mainly explore its role in the biosynthesis of coenzyme A (CoA) and highlight its potential as a target in pantothenate kinase-associated neurodegeneration (PKAN) disorders (16–19). Nevertheless, PANK4 also appears to possess additional roles beyond those already described. Notably, PANK4 is characterised by a DUF89 phosphatase domain that appears to be central to PANK4 function. Intriguingly, the DUF89 domain was reported to confer to the protein its unique features as damage-control phosphatase, being responsible for clearing the cells from unwanted normal or damaged metabolites that can build up to toxic levels under certain conditions (17). It is worth mentioning that based on the principle of "guilt by association" (50), the domains of fusion proteins are likely to be functionally related. This is probably why, considering PANKs' involvement in CoA biosynthesis, studies have mostly focused their efforts to investigate the role of PANK4 in the CoA pathway (16–19).

Our findings suggest that PANK4 could have broader functions by controlling the levels of a wider range of toxic molecules, including but not limited to reactive oxygen species (ROS). To note, a number of metabolites can exert toxic effects and, if not promptly 'drained', can accumulate to toxic levels (39). Our proteomic analysis uncovered a marked downregulation of a host of detoxification proteins in response to PANK4 silencing, such as GSTP1, NQO1, PRDX3, PRDX1, ADH5, SRXN1, DHFR, GSTM2, ESD, ALDH1A1, GSTM3, MTARC2, AKR1B10, PARK7, some of which play crucial roles in cellular protection against oxidative stress in GBM (30–35, 51) and other cancers (37, 38, 40–42). In line with other studies, downregulation of the above-mentioned proteins has been linked to numerous processes in GBM, such as inhibition of cell proliferation and tumour growth (30–34, 51–53) increased apoptosis (31, 32, 35, 51, 52)

and most importantly, sensitisation of GBM cells to treatment with TMZ and/or ionizing radiation (30, 33, 35, 36, 53). Similar effects have also been observed in other cancer types (41, 54, 55).

Interestingly, we also showed that PANK4 expression is induced in TMZ-resistant GBM cells following exposure to the drug, suggesting a potential requirement for PANK4 in the response to TMZ-induced genotoxic damage. Notably, the DUF89 gene YMR027W in yeast has been reported to be upregulated in response to treatment with the DNA-damaging agent methyl methanesulfonate (17, 56, 57). Similarly, its human ortholog, C6orf211 (Armt1), has also been implicated in the response to DNA damage (58).

As cancer cells depend on several compensatory mechanisms, especially following potential accumulation of lethal damage, the increase in PANK4 levels after TMZ treatment could provide an advantage to GBM cells. Herein, we propose a mechanism whereas PANK4 depletion compromises the detoxification response in TMZ-resistant GBM cells, as demonstrated by the downregulation of a number of cellular detoxification proteins. This, alongside the genotoxic stress induced by TMZ leads to a crucial perturbation of the cellular damage response, culminating to cell death (Fig. 8). Nevertheless, much still needs to be learnt about PANK4, and the extent of its involvement in the cellular detoxification mechanisms at the molecular level has yet to be fully defined. A comprehensive profiling of the implicated toxic metabolites may guide future research efforts and uncover metabolic signatures and vulnerabilities for drug-resistant GBM cells. Leveraging such synthetic vulnerabilities can prove crucial to reverse chemoresistance and restore sensitivity to TMZ, therefore representing a valuable strategy to improve GBM patients' response to TMZ treatment.

Conclusions

Our study provides novel insights into chemoresistance in GBM and unveils a protective role for PANK4 in TMZ-resistant cells. More specifically, in light of the involvement of PANK4 in the cellular detoxification response, depletion of the protein crucially shifts the balance towards an impaired stress response, exacerbating the damage caused by TMZ and ultimately leading to cell death. In summary, PANK4 represents a synthetic vulnerability that could be exploited to restore sensitivity to the drug.

Abbreviations

TMZ: temozolomide

GBM: glioblastoma

PANK4: pantothenate kinase 4

TMT: tandem mass tag

CNS: central nervous system

DUF89: c-terminal phosphatase domain

OS: overall survival

RCCL: Resistant Cancer Cell Line collection

HGCC: the Human Glioblastoma Cell Culture biobank

Declarations

Ethical Approval

All animal studies were performed in full compliance with FELASA (Federation of Laboratory Animal Science Associations) recommendations in the Animal House Facility of the Biomedical Research Foundation of the Academy of Athens (BRFAA, Greece). All procedures for the care and treatment of the animals were approved by the Institutional Committee on Ethics of Animal Experiments. The license for the animal handling protocol for this project is: 1385947/27-12-2022.

Clinical GBM specimens (n= 79 GBM, IDH-wildtype patients) were collected in the cancer centre at Renmin Hospital of Wuhan University, and processed at the hospital research laboratories after de-identification of the samples.The study was approved by the ethics committee of Renmin Hospital of Wuhan University (March 15th, 2022). The approval number is: WDRY2022-K064.

Competing interests

Georgios Giamas is the Founder/Chief Scientific Officer of StingrayBio and an Associate Editor in Oncogene. Justin Stebbing conflicts are listed at https://www.nature.com/onc/editors. The remaining authors declare that they have no conflict of interest.

Authors' contributions

Methodology: V.V., A.D., A.C., T.G., C.B.; data analysis: V.V., A.C., M.E., S.K.W., E.K., F.M.G.P., L.P., A.K.; collection and IHC staining of clinical specimens: L.P., B.X., Y.Z.; IHC analysis and scoring: GL; writing and editing: V.V., J.S., G.G.; supervision: G.G.; funding acquisition, G.G. All authors have read and agreed to the published version of the manuscript.

Funding

This research was funded by Action Against Cancer, grant number ID9087/G2467.

Availability of data and materials

All relevant data are available from the authors upon request. The TMT-based proteomics data have been deposited to the ProteomeXchange Consortium (http://www.proteomexchange.org) (59) via the PRIDE (60) partner repository with the dataset identifier PXD040871 and 10.6019/PXD040871.

Acknowledgements

The TMZ-resistant GBM cancer cell lines (U87MG^{Res}, T98G^{Res} and LN229^{Res}) and their parental counterparts (U87MG^{Par}, T98G^{Par} and LN229^{Par}) were kindly provided by Prof. Martin Michaelis [the Resistant Cancer Cell Line (RCCL) collection, University of Kent, UK]. The U251^{Res} and U251^{Par} cell lines were kindly provided by Dr Corinne Griguer (University of Iowa, USA). Primary GBM cell lines were kindly provided by Dr Lene Uhrbom [the Human Glioblastoma Cell Culture (HGCC) biobank, Uppsala University, Sweden]. The TMT-based proteomic experiment was performed by DC Biosciences (https://dcbiosci.com). Figure 6A and Figure 6B were generated based on data derived from the Rembrandt brain cancer dataset (https://gdoc.georgetown.edu) (26). Figure 6D and Figure 6E were based on data available at the Gene Expression Omnibus (GEO; www.ncbi.nlm.nih.gov/geo, accession number: GSE68029) (28). The graphical abstract, figures 1A, 4D, 5A, 6I, 7A and 7G were created with BioRender.com.

Materials And Methods

Reagents

TMZ (#T2577-25MG) was purchased from Sigma-Aldrich and resuspended in DMSO (ThermoFisher Scientific, #D/4125/PB08). PANK4 (#12055, 1:1000), MCL1 (#5453, 1:1000), caspase-3 (#9665, 1:1000), cleaved caspase-3 (#9664, 1:1000), GAPDH (#5174, 1:1000) as well as anti-rabbit (#7074P2, 1:4000) and anti-mouse (#7076P2, 1:4000) HRP-linked antibodies were purchased from Cell Signaling Technology. Alpha-tubulin (#A01410-100, 1:1000) was purchased from GenScript. The anti-Ki-67 antibody (#ab15580, 1:150) was purchased from Abcam and the anti-PANK4 antibody (#HPA027961, 1:300)was purchased from Sigma-Aldrich. The pCMV6-PANK4 overexpressing plasmid (#RC208116) and the pCMV6 empty vector (#PS100001) were purchased from Origene. The pLKO.1-puro PANK4 shRNA (#SH0111; targeting sequence: GGACTCTTCTGCTTGTCACTT) and the pLKO.1-puro non-targeting scrambled shRNA (#SHC016) were purchased from Sigma-Aldrich. The pMD2.G (#12259) and psPAX2 (#12260) packaging plasmids were obtained from Addgene. All other reagents, if not otherwise specified, were purchased from ThermoFisher Scientific.

Cell lines and culture conditions

The TMZ-resistant GBM cell lines (U87MG^{Res}, T98G^{Res} and LN229^{Res}) and their parental counterparts (U87MG^{Par}, T98G^{Par} and LN229^{Par}) used in this study were derived from the “Resistant Cancer Cell Line (RCCL) collection” (https://research.kent.ac.uk/industrial-biotechnology-centre/the-resistant-cancer-cell-line-rccl-collection/; University of Kent, UK) (21) and established by continuous exposure to increasing drug concentrations as described before (61). These cell lines as well as the control and stably PANK4-depleted T98G^{Res} cells were cultured in Iscove's Modified Dulbecco's Medium(IMDM; ThermoFisher Scientific, #21980-032)supplemented with 10% fetal bovine serum (FBS; Sigma-Aldrich, #F7524-500ML), 1% Penicillin-Streptomycin solution (Sigma-Aldrich, #P0781-100ML) and 4mM L-glutamine (Sigma-

Aldrich, #G7513). The U251^{Res} and U251^{Par} cell lines were kindly provided by Dr Corinne Griguer (University of Iowa, Iowa City, USA) and were generated as previously described (22). These cells were grown in DMEM/F-12 medium (ThermoFisher Scientific, #11320-033) supplemented with 7% heat-inactivated FBS (Sigma-Aldrich, #F7524-500ML) and 1% Penicillin-Streptomycin solution (Sigma-Aldrich, #P0781-100ML). All drug-resistant cells mentioned above were maintained in culture in the presence of TMZ as previously described (https://research.kent.ac.uk/industrial-biotechnology-centre/the-resistant-cancer-cell-line-rccl-collection/) (21, 22). The U3027MG and U3031MG patient-derived GBM cell lines were obtained from the “Human Glioblastoma Cell Culture (HGCC) biobank” (https://www.hgcc.se; Uppsala University, Uppsala, Sweden) (23). These cell lines were cultured in Neurobasal (ThermoFisher Scientific, # 21103-049) and DMEM/F-12 GlutaMAX (ThermoFisher Scientific, #31331-028) medium (1:1), supplemented with B-27 (ThermoFisher Scientific, #12587010), N2 (ThermoFisher Scientific, #17502048), EGF (PeproTech, #AF-100-15-100UG), FGF (PeproTech, #100-18B-100UG), 1% Penicillin-Streptomycin solution (Sigma-Aldrich, #P0781-100ML) and grown on laminin-coated Corning Primaria Cell Culture plates (Corning, #353846 & 353872), as previously described (23). HEK-293T cells were purchased from ATCC and maintained in Dulbecco's Modified Eagle's Medium (DMEM; Sigma-Aldrich, #D6046-500ML) supplemented with 10% FBS (Sigma-Aldrich, #F7524-500ML) and 1% Penicillin-Streptomycin solution (Sigma-Aldrich, #P0781-100ML). All cell lines were incubated at 37°C with 5% CO_2 and regularly subjected to *mycoplasma* testing.

Kinome-wide RNAi screen

The “Silencer Select Human Kinase siRNA Library V4” (ThermoFisher Scientific, #4397918), targeting 709 human kinase and kinase-related genes was used. U87MG^{Res} cells (3000/well) were reverse transfected in 96-well plates with either a pool of 3 siRNAs targeting each gene of the library (25nM/siRNA) or non-targeting negative control siRNAs (ThermoFisher Scientific, #4390844). The Lipofectamine 3000 transfection reagent (ThermoFisher Scientific, #L3000015) was used according to the manufacturer’s instructions. 24 hours after transfection, cells were treated with either DMSO or a sublethal dose of TMZ (IC_{20}), and incubated for 96 hours. Cell proliferation was determined using the CyQUANT Direct assay (ThermoFisher Scientific, #C35011), following the manufacturer’s instructions. Two independent primary screens (biological repeats) were performed. Data were background corrected and normalised to their respective control (siCTRL DMSO). Normalised values were used to calculate z-scores as previously described (62). Gene candidates displaying an effect of >20% on cell proliferation alone were excluded from further analysis.

PANK4 silencing and overexpression

Cells were reverse transfected with a pool of 3 siRNAs (25nM each) using the Lipofectamine 3000 transfection reagent (ThermoFisher Scientific, #L3000015), according to the manufacturer’s instructions. Non-targeting negative control siRNA (ThermoFisher Scientific, #4390843) and PANK4 siRNAs (ThermoFisher Scientific, #4392420; IDs: s224353, s30501, s30502) were used. Briefly, a mix of siRNAs, Opti-MEM medium (ThermoFisher Scientific, #31985062) and Lipofectamine 3000 was prepared

following the manufacturer's instructions. After formation of the transfection complexes, the transfection mix was spotted into the wells and cells were subsequently seeded. For PANK4 overexpression, cells were seeded into wells and transfected with the pCMV6-PANK4 overexpressing plasmid (Origene, #RC208116) or the pCMV6 empty vector (Origene, #PS100001), using the Fugene HD transfection reagent (Promega, #E2311), according to the manufacturer's instructions. To achieve long-term PANK4 knockdown, lentiviral-mediated shRNA transfection was performed. Briefly, HEK-293T cells were transiently co-transfected with pLKO.1-puro PANK4 shRNA (targeting sequence: GGACTCTTCTGCTTGTCACTT) (Sigma-Aldrich, #SH0111) or pLKO.1-puro non-targeting scrambled shRNA (Sigma-Aldrich, #SHC016), and pMD2.G, psPAX2 packaging plasmids (Addgene, #12259 and #12260, respectively). Transient transfection was performed using Lipofectamine 3000 (ThermoFisher Scientific, #L3000015), as described above. Non-replicating viral particles were harvested and concentrated using PEG-it (5x) (System Biosciences, #LV810A-1) overnight at 4°C. The concentrated virus was dispensed to $T98G^{Res}$ cells, and TransDux (200x) (System Biosciences, #LV850A-1) was added to increase transduction efficiency. 72-hours post transduction, cells were incubated in the presence of 0.8 µg/mL puromycin (Gibco, #A1113803) to ensure effective positive selection. For all the experiments performed, PANK4 silencing and overexpression were confirmed by western blotting, as indicated in the respective figure legends.

Cell proliferation assays

Briefly, cells were reverse transfected with siCTRL or siPANK4, as described above. After 24 hours, cells were treated with DMSO or TMZ, as specified in the figures and their respective legends. Cell proliferation was evaluated by the CyQUANT Direct assay (ThermoFisher Scientific, #C35011), following the manufacturer's instructions. Fluorescence intensity was measured on a SpectraMax i3x microplate reader (Molecular Devices). Alternatively, the crystal violet assay was used. Following fixation of cells with 4% paraformaldehyde solution (Santa Cruz Biotechnology, #sc-281692) in 1x PBS, and staining with 0.5% crystal violet (ThermoFisher Scientific, #B21932.14), absorbance was measured using the GloMax-Multi detection system (Promega).

Clonogenic survival assays

Clonogenic survival assays were performed as previously described (63, 64). Briefly, cells were transfected with either siCTRL or siPANK4 and subsequently seeded at predetermined densities. After 24 hours, cells were treated with DMSO or TMZ, as indicated. When colony size reached more than 50 cells per colony, cells were fixed with 4% paraformaldehyde solution (Santa Cruz Biotechnology, #sc-281692) in 1x PBS, followed by staining with 0.5% crystal violet (ThermoFisher Scientific, #B21932.14). The surviving fraction was determined using the plating efficiencies of the respective controls as reference.

Cell death and apoptosis

The assay was performed as previously described (65, 66). Cells were transfected with either siCTRL or siPANK4 as described above and subjected to drug treatments as specified in the corresponding figures

and figure legends. After 96 hours, cells were stained using the Muse Annexin V Dead Cell Kit according to the manufacturer's instructions (Luminex, #MCH100105). Cells were then analysed using the Muse Cell Analyzer (Millipore).

ROS detection

The assay was performed using the DCFDA / H2DCFDA - Cellular ROS Assay Kit (Abcam, #ab113851). Briefly, cells were transfected with either siCTRL or siPANK4 as described above and treated with a sublethal concentration of TMZ, as previously determined. After 96 hours cells were stained with DCFDA solution according to the manufacturer's instructions and fluorescence was measured using the BMG Labtech CLARIOstar Microplate Reader at Ex/Em = 485/535 nm.

RNA extraction and RT-qPCR

Total RNA was extracted using the PureLink RNA Mini Kit (Invitrogen, #12183018A) following the manufacturer's instructions (62, 67). All RNA samples were subjected to DNase treatment. The concentration and purity of RNA was determined using a Nanodrop 2000 spectrophotometer (ThermoFisher Scientific). Complementary DNA (cDNA) synthesis was performed using the High-Capacity cDNA Reverse Transcription Kit according to the manufacturer's instructions (ThermoFisher Scientific #4368814). Quantitative real-time PCR was carried out using the SYBR green gene expression assay (Applied Biosystems, #4367659). Samples were run on a StepOne thermal cycler (Applied Biosystems) and analyzed with the SDS 1.9 software (Applied Biosystems) (n = 3 biological replicates and n = 3 technical replicates). GAPDH was used as an internal control. Primer sequences are listed in **Supplementary Table S4**.

Western Blotting

Western Blotting was performed as previously described (62, 65, 68). Briefly, cells were lysed in RIPA buffer (Sigma-Aldrich, #R0278) supplemented with protease and phosphatase inhibitors (Roche, #11697498001 and #4906845001, respectively). Protein concentration was determined using the Pierce BCA protein assay kit (ThermoFisher Scientific, #23227). Proteins were resolved by SDS-PAGE and transferred onto a nitrocellulose transfer membrane (ThermoFisher Scientific, #IB23001) using the iBlot 2 dry blotting system (ThermoFisher Scientific, #IB21001). Following blocking of membranes in TBS containing 0.1% (v/v) Tween 20 and 5% (w/v) non-fat milk for 1 hour, incubation with primary antibodies was performed overnight at 4°C. Anti-mouse (#7076P2, 1:4000) and anti-rabbit (#7074P2, 1:4000) horseradish peroxidase (HRP)-conjugated secondary antibodies were used (Cell Signaling Technology) and binding was detected using the SuperSignal West Pico PLUS chemiluminescent substrate (ThermoFisher Scientific, #34577). Emission was captured using the UVP ChemStudio Imaging Systems (Analityk jena). Densitometric analysis of western blots was performed using the ImageJ software.

Animal experiments

NOD.Cg-Prkdcscid Il2rgtm1Wjl/SzJ (stock no: 005557; NSG) (69, 70) mice were purchased from the Jax repository (Bar Harbor, ME, USA) and bred in-house in individually ventilated cages under specific pathogen-free conditions. All animal studies were performed in full compliance with FELASA (Federation of Laboratory Animal Science Associations) recommendations in the Animal House Facility of the Biomedical Research Foundation of the Academy of Athens (BRFAA, Greece). All procedures for the care and treatment of the animals were approved by the Institutional Committee on Ethics of Animal Experiments. The license for the animal handling protocol for this project is: 1385947/27-12-2022. To produce the ectopic tumour xenograft model, $10x10^6$ $T98G^{Res}$ cells in 10% matrigel (Corning) were subcutaneously injected in the right and left flank of mice. After establishing palpable tumours (~30 mm^3), mice were randomly assigned to groups. Tumour volume was measured twice a week with caliper and calculated as $V=axb^2/2$, “a” being the largest diameter, “b” the smallest. Tumour specimens up to 50 mm^3 from non-treated mice were transplanted subcutaneously in new NSG mice under anaesthesia in order to produce mirror images of the primary tumour.

In vivo transfections

In Vivo Ready non-targeting negative control siRNA (ThermoFisher Scientific, #4404020) and PANK4 siRNAs (ThermoFisher Scientific, #4404010; HPLC-IVR IDs: s224353, s30501) were used in this study. siRNAs were encapsulated using Invivofectamine 3.0 reagent (ThermoFisher Scientific, #IVF3001), a cationic liposome-based formulation, according to the manufacturer’s instructions. Animals were anesthetized using an intraperitoneal injection of ketamine (100 mg/kg) and xylazine (12 mg/kg). The injection site was swabbed with 70% ethanol prior to injection. siRNA:Invivofectamine 3.0 complexes were injected intratumorally at a concentration of 6μg/tumour at day 1 and 5. The siRNA concentrations used were based on previously published studies (71, 72) and knockdown efficiency was assessed by western blot.

In vivo TMZ treatments

TMZ (MedChemExpress, #HY-17364/CS-0943) was administered intraperitoneally (IP) at a concentration of 1.5mg/kg on day 2 and every other day for the following 12 days. The concentration of TMZ used was based on the dose response curve generated after IP administration of TMZ at concentrations of 0 (vehicle), 1, 3 and 10 mg/kg. TMZ was dissolved in 5% DMSO / 5% solutol (Sigma-Aldrich) in PBS. At the end of each treatment, mice were euthanized in accordance with standard protocols. A small part of the freshly dissected tumour was fresh frozen for molecular analysis and the rest was fixed in a 10% formalin solution.

Immunoblotting of xenograft tumour tissues

Tumours were lysed in 8M UREA/50mM TEAB with protease inhibitors (Calbiochem) using mild sonication on ice followed by homogenization with a 26 G syringe. Total protein concentration was determined with the Bio-Rad protein assay. Lysates were subjected to SDS-PAGE followed by immunoblot analysis. The primary antibodies used were PANK4 (Cell Signaling Technology, #12055, 1:1000) and

GAPDH (Cell Signaling Technology, #5174, 1:1000). The anti-rabbit HRP-conjugated secondary antibody (Cell Signaling Technology) was used at a 1:4000 dilution. Densitometric analysis of western blots was performed using the ImageJ software.

Immunohistochemistry of xenograft tumour tissues

Immunohistochemistry (IHC) was performed according to standard procedures (65, 73). Rabbit anti-Ki-67 antibody (Abcam, #ab15580, 1:150) was used for overnight incubation at 4°C in humidified chambers. The anti-rabbit secondary antibody (Cell Signaling Technology, 1:400) was HRP-conjugated and was detected with DAB (Vector Laboratories).

Immunohistochemical analysis of clinical specimens

Immunohistochemistry staining for PANK4 and hematoxylin and eosin (H&E) staining were performed as previously described (65, 74, 75). The anti-PANK4 antibody (Sigma-Aldrich, #HPA027961) was used at a 1:300 dilution. The study was approved by the ethics committee of Renmin Hospital of Wuhan University (March 15th, 2022). The approval number is: WDRY2022-K064. Clinical GBM specimens (n= 79 GBM, IDH-wildtype patients) were collected in the cancer centre at Renmin Hospital of Wuhan University, and processed at the hospital research laboratories after de-identification of the samples. PANK4 immunoreactivity was assessed semi-quantitatively on a 0-2 scale, with 0=negative, 1+=mild, 2+=moderate staining (https://www.proteinatlas.org). Percentages of 0, 1+, 2+ cells were recorded. H-scores were calculated as follows: % of (1+) cells + 2x[% of (2+) cells]. All cases were scored without knowledge of the clinicopathological data. Patients' information is provided in **Supplementary Table S5**.

Sample preparation for the TMT-based proteomic experiment

Briefly, T98G^{Res} cells were reverse transfected with either siCTRL or siPANK4. After 24 hours, cells were treated with either DMSO or TMZ. Following 96h, cells were washed (×3 in PBS) and pelleted. Cell pellets were lysed separately with freshly prepared lysis buffer containing 50 mM HEPES, pH 8.0, 2% SDS, 1 mM PMSF, supplemented with phosphatase and protease inhibitor cocktail (Sigma-Aldrich). Samples were thawed at room temperature (RT) for 20 minutes (min) before heating to 99°C for 5 min. After cooling to RT, DNA was sheared by sonication. Cell debris was removed by centrifugation at 20,000×g for 15 min at 20 °C. Protein concentration was determined using the BCA protein assay kit (Applichem GmbH, Darmstadt, Germany).

Protein digestion and offline fractionation

FASP digestion was performed according to the procedure described by Wisniewski *et al*. (76). TMT labelling was performed with TMTpro 16-plex reagents (Lot#WA314599) according to the manufacturer's instructions (Pierce, Rockford, IL, USA). Offline Fractionation of peptides into 12 fractions was performed via RP-HPLC at high pH as described by Gilar *et al*. (77). After solvent removal in a vacuum concentrator, samples were reconstituted in 0.1% TFA for LC-MS/MS analysis.

Liquid chromatography-mass spectrometry analysis

Mass spectrometry was performed on an Orbitrap Fusion Lumos mass spectrometer (ThermoFisher Scientific, San Jose, CA, USA) coupled to a Dionex Ultimate 3000RSLC nano system (ThermoFisher Scientific, San Jose, CA, USA) via a nanoflex source. Tryptic peptides were separated on a 50 cm, 75 µm i.d. analytical column (self-packed with ReproSil-Pur 120 C18-AQ, 3 µm, Dr. Maisch, Ammerbuch Entringen, Germany) and a 90 min acetonitrile gradient (5-90%) at a flow rate of 230 nL/min. Analysis was performed in a data-dependent acquisition mode using a TopN dependent scan method with a cycle time of up to 20 scans for precursor ion selection. MS1 data were acquired in the orbitrap at a resolution of 120,000 (at 200 m/z). Automatic gain control (AGC) was set to a target of 2.5E4 and a maximum injection time of 86 ms. MS2 spectra were acquired in the orbitrap (FT) using a quadrupole isolation window of 0.5 Da and higher-energy collision induced dissociation (HCD) at a normalised collision energy (NCE) of 34%. The resolution was 50,000 (at 200 m/z) with a fixed first mass of 110 m/z, an AGC target of 5E4, and a maximum injection time of 110 ms. Dynamic exclusion for selected ions was 90 s. A single lock mass at m/z 445.120024 was employed (78).

Proteomic data analysis

Protein identification and comparative quantification of TMTpro 16-plex labelled proteins from MS and MS/MS raw data were performed using the MaxQuant software suit (version 1.6.12.0) (Max Planck Institute of Biochemistry, Planegg, Germany) with the implemented peptide search engine Andromeda (79) against a reference proteome database of Homo sapiens (Human/Uniprot proteome ID: UP000005640, Version 7 March 2021). Statistical analysis was performed using the Perseus software (version 1.6.14.0). Unpaired t-test was employed to determine the significance of the observed differences. Differences were considered statistically significant at $p < 0.05$ (95% confidence interval, * $p < 0.05$; ** $p < 0.01$; *** $p < 0.001$; **** $p < 0.0001$).

Gene Set Enrichment Analysis

Functional annotation and Gene Set Enrichment Analysis (GSEA) were performed using clusterProfiler (v 4.4.4) (80). Enrichment representations were plotted with the dotplot, cnetplot and gseaplot2 functions. Gene Ontology (GO) terms were considered significantly enriched in over-representation analysis when Benjamini-Hochberg adjusted *p* values were below < 0.05(*). For all analyses and plots, R (v 4.2.0) and Bioconductor (v 3.15) were used.

Statistical analysis

Graphics and statistical analysis were performed using the GraphPad Prism 9 software. Each experiment was conducted at least three times and results are expressed as mean ± SEM, unless otherwise specified. Statistical significance was evaluated using unpaired Student's t-test when two groups were compared. More than two groups were compared using two-way ANOVA, unless otherwise specified. For assessment of biological reproducibility of the two primary screens, correlation was determined using the Pearson

correlation coefficient. The Cooperativity Index (CI) was calculated as previously described (81). CI values < 1 indicate a synergistic effect, when CI values = 1 the effect is additive, and CI values > 1 indicate an antagonistic effect. The statistical significance of the Kaplan-Meier survival plots was evaluated by log-rank analysis. The statistical details and *p*-values of each experiment are indicated in the corresponding figures and figure legends [p-values: *$p < 0.05$, **p < 0.01, ***$p < 0.001$, ****$p < 0.0001$ and “ns” indicates not significant ($p>0.05$)].

References

1. McKinnon C, Nandhabalan M, Murray SA, Plaha P. Glioblastoma: clinical presentation, diagnosis, and management. Bmj. 2021;374:n1560.
2. Alexander BM, Cloughesy TF. Adult Glioblastoma. J Clin Oncol. 2017;35(21):2402-9.
3. Campos B, Olsen LR, Urup T, Poulsen HS. A comprehensive profile of recurrent glioblastoma. Oncogene. 2016;35(45):5819-25.
4. Krause DS, Van Etten RA. Tyrosine kinases as targets for cancer therapy. N Engl J Med. 2005;353(2):172-87.
5. Giamas G, Man YL, Hirner H, Bischof J, Kramer K, Khan K, et al. Kinases as targets in the treatment of solid tumors. Cell Signal. 2010;22(7):984-1002.
6. Comprehensive genomic characterization defines human glioblastoma genes and core pathways. Nature. 2008;455(7216):1061-8.
7. Brennan CW, Verhaak RG, McKenna A, Campos B, Noushmehr H, Salama SR, et al. The somatic genomic landscape of glioblastoma. Cell. 2013;155(2):462-77.
8. Rodgers G, Austin C, Anderson J, Pawlyk A, Colvis C, Margolis R, et al. Glimmers in illuminating the druggable genome. Nat Rev Drug Discov. 2018;17(5):301-2.
9. Essegian D, Khurana R, Stathias V, Schürer SC. The Clinical Kinase Index: A Method to Prioritize Understudied Kinases as Drug Targets for the Treatment of Cancer. Cell Rep Med. 2020;1(7):100128.
10. Vella V, Giamas G, Ditsiou A. Diving into the dark kinome: lessons learned from LMTK3. Cancer Gene Ther. 2022;29(8-9):1077-9.
11. Sheetz JB, Lemmon MA. Looking lively: emerging principles of pseudokinase signaling. Trends Biochem Sci. 2022;47(10):875-91.
12. Kung JE, Jura N. Prospects for pharmacological targeting of pseudokinases. Nat Rev Drug Discov. 2019;18(7):501-26.
13. Jacobsen AV, Murphy JM. The secret life of kinases: insights into non-catalytic signalling functions from pseudokinases. Biochem Soc Trans. 2017;45(3):665-81.
14. Zhang H, Photiou A, Grothey A, Stebbing J, Giamas G. The role of pseudokinases in cancer. Cell Signal. 2012;24(6):1173-84.
15. Stebbing J, Zhang H, Xu Y, Lit LC, Green AR, Grothey A, et al. KSR1 regulates BRCA1 degradation and inhibits breast cancer growth. Oncogene. 2015;34(16):2103-14.

16. Yao J, Subramanian C, Rock CO, Jackowski S. Human pantothenate kinase 4 is a pseudo-pantothenate kinase. Protein Sci. 2019;28(6):1031-47.
17. Huang L, Khusnutdinova A, Nocek B, Brown G, Xu X, Cui H, et al. A family of metal-dependent phosphatases implicated in metabolite damage-control. Nat Chem Biol. 2016;12(8):621-7.
18. Dibble CC, Barritt SA, Perry GE, Lien EC, Geck RC, DuBois-Coyne SE, et al. PI3K drives the de novo synthesis of coenzyme A from vitamin B5. Nature. 2022;608(7921):192-8.
19. Munshi MI, Yao SJ, Ben Mamoun C. Redesigning therapies for pantothenate kinase-associated neurodegeneration. J Biol Chem. 2022;298(3):101577.
20. Linster CL, Van Schaftingen E, Hanson AD. Metabolite damage and its repair or pre-emption. Nat Chem Biol. 2013;9(2):72-80.
21. Michaelis M, Wass MN, Cinatl J. Drug-adapted cancer cell lines as preclinical models of acquired resistance. Cancer Drug Resist. 2019;2(3):447-56.
22. Oliva CR, Nozell SE, Diers A, McClugage SG, 3rd, Sarkaria JN, Markert JM, et al. Acquisition of temozolomide chemoresistance in gliomas leads to remodeling of mitochondrial electron transport chain. J Biol Chem. 2010;285(51):39759-67.
23. Xie Y, Bergström T, Jiang Y, Johansson P, Marinescu VD, Lindberg N, et al. The Human Glioblastoma Cell Culture Resource: Validated Cell Models Representing All Molecular Subtypes. EBioMedicine. 2015;2(10):1351-63.
24. Wang H, Guo M, Wei H, Chen Y. Targeting MCL-1 in cancer: current status and perspectives. J Hematol Oncol. 2021;14(1):67.
25. Shalini S, Dorstyn L, Dawar S, Kumar S. Old, new and emerging functions of caspases. Cell Death Differ. 2015;22(4):526-39.
26. Gusev Y, Bhuvaneshwar K, Song L, Zenklusen JC, Fine H, Madhavan S. The REMBRANDT study, a large collection of genomic data from brain cancer patients. Sci Data. 2018;5:180158.
27. Liu Y, Cheng Z, Li Q, Pang Y, Cui L, Qian T, et al. Prognostic significance of the PANK family expression in acute myeloid leukemia. Ann Transl Med. 2019;7(12):261.
28. Tso JL, Yang S, Menjivar JC, Yamada K, Zhang Y, Hong I, et al. Bone morphogenetic protein 7 sensitizes O6-methylguanine methyltransferase expressing-glioblastoma stem cells to clinically relevant dose of temozolomide. Mol Cancer. 2015;14:189.
29. Alafate W, Xu D, Wu W, Xiang J, Ma X, Xie W, et al. Loss of PLK2 induces acquired resistance to temozolomide in GBM via activation of notch signaling. J Exp Clin Cancer Res. 2020;39(1):239.
30. Svendsen A, Verhoeff JJ, Immervoll H, Brøgger JC, Kmiecik J, Poli A, et al. Expression of the progenitor marker NG2/CSPG4 predicts poor survival and resistance to ionising radiation in glioblastoma. Acta Neuropathol. 2011;122(4):495-510.
31. Lei K, Gu X, Alvarado AG, Du Y, Luo S, Ahn EH, et al. Discovery of a dual inhibitor of NQO1 and GSTP1 for treating glioblastoma. J Hematol Oncol. 2020;13(1):141.

32. Xu Z, Zeng X, Li M, Liao J, Chen Q. MicroRNA-383 promotes reactive oxygen species-induced autophagy via downregulating peroxiredoxin 3 in human glioma U87 cells. Exp Ther Med. 2021;21(5):439.
33. Schäfer A, Teufel J, Ringel F, Bettstetter M, Hoepner I, Rasper M, et al. Aldehyde dehydrogenase 1A1–a new mediator of resistance to temozolomide in glioblastoma. Neuro Oncol. 2012;14(12):1452-64.
34. Lei K, Xia Y, Wang XC, Ahn EH, Jin L, Ye K. C/EBPβ mediates NQO1 and GSTP1 anti-oxidative reductases expression in glioblastoma, promoting brain tumor proliferation. Redox Biol. 2020;34:101578.
35. Kim JY, Kim HJ, Jung CW, Choi BI, Lee DH, Park MJ. PARK7 maintains the stemness of glioblastoma stem cells by stabilizing epidermal growth factor receptor variant III. Oncogene. 2021;40(3):508-21.
36. Cheng SY, Chen NF, Wen ZH, Yao ZK, Tsui KH, Kuo HM, et al. Glutathione S-Transferase M3 Is Associated with Glycolysis in Intrinsic Temozolomide-Resistant Glioblastoma Multiforme Cells. Int J Mol Sci. 2021;22(13).
37. Liu Y, Zhang J, Liu H, Guan G, Zhang T, Wang L, et al. Compensatory upregulation of aldo-keto reductase 1B10 to protect hepatocytes against oxidative stress during hepatocarcinogenesis. Am J Cancer Res. 2019;9(12):2730-48.
38. Lv X, Yu H, Zhang Q, Huang Q, Hong X, Yu T, et al. SRXN1 stimulates hepatocellular carcinoma tumorigenesis and metastasis through modulating ROS/p65/BTG2 signalling. J Cell Mol Med. 2020;24(18):10714-29.
39. Lee N, Spears ME, Carlisle AE, Kim D. Endogenous toxic metabolites and implications in cancer therapy. Oncogene. 2020;39(35):5709-20.
40. An Y, Jiang J, Zhou L, Shi J, Jin P, Li L, et al. Peroxiredoxin 1 is essential for natamycin-triggered apoptosis and protective autophagy in hepatocellular carcinoma. Cancer Lett. 2021;521:210-23.
41. Chen HC, Long M, Gao ZW, Liu C, Wu XN, Yang L, et al. Silencing of B7-H4 induces intracellular oxidative stress and inhibits cell viability of breast cancer cells via downregulating PRDX3. Neoplasma. 2022;69(4):940-7.
42. Singh RR, Mohammad J, Orr M, Reindl KM. Glutathione S-Transferase pi-1 Knockdown Reduces Pancreatic Ductal Adenocarcinoma Growth by Activating Oxidative Stress Response Pathways. Cancers (Basel). 2020;12(6).
43. Chen J, Li Y, Yu TS, McKay RM, Burns DK, Kernie SG, et al. A restricted cell population propagates glioblastoma growth after chemotherapy. Nature. 2012;488(7412):522-6.
44. Uribe D, Torres Á, Rocha JD, Niechi I, Oyarzún C, Sobrevia L, et al. Multidrug resistance in glioblastoma stem-like cells: Role of the hypoxic microenvironment and adenosine signaling. Mol Aspects Med. 2017;55:140-51.
45. Jackson CM, Choi J, Lim M. Mechanisms of immunotherapy resistance: lessons from glioblastoma. Nat Immunol. 2019;20(9):1100-9.
46. Lang F, Liu Y, Chou FJ, Yang C. Genotoxic therapy and resistance mechanism in gliomas. Pharmacol Ther. 2021;228:107922.

47. Mayoral-Varo V, Jiménez L, Link W. The Critical Role of TRIB2 in Cancer and Therapy Resistance. Cancers (Basel). 2021;13(11).
48. Haikala HM, Jänne PA. Thirty Years of HER3: From Basic Biology to Therapeutic Interventions. Clin Cancer Res. 2021;27(13):3528-39.
49. Passirani C, Vessières A, La Regina G, Link W, Silvestri R. Modulating undruggable targets to overcome cancer therapy resistance. Drug Resist Updat. 2022;60:100788.
50. Suhre K. Inference of gene function based on gene fusion events: the rosetta-stone method. Methods Mol Biol. 2007;396:31-41.
51. Li G, Cai Y, Wang C, Huang M, Chen J. LncRNA GAS5 regulates the proliferation, migration, invasion and apoptosis of brain glioma cells through targeting GSTM3 expression. The effect of LncRNA GAS5 on glioma cells. J Neurooncol. 2019;143(3):525-36.
52. Jin S, Dai Y, Li C, Fang X, Han H, Wang D. MicroRNA-544 inhibits glioma proliferation, invasion and migration but induces cell apoptosis by targeting PARK7. Am J Transl Res. 2016;8(4):1826-37.
53. Zhao M, Tan B, Dai X, Shao Y, He Q, Yang B, et al. DHFR/TYMS are positive regulators of glioma cell growth and modulate chemo-sensitivity to temozolomide. Eur J Pharmacol. 2019;863:172665.
54. Qu J, Li J, Zhang Y, He R, Liu X, Gong K, et al. AKR1B10 promotes breast cancer cell proliferation and migration via the PI3K/AKT/NF-κB signaling pathway. Cell Biosci. 2021;11(1):163.
55. Lin JH, Tu SH, Chen LC, Huang CC, Chang HL, Cheng TC, et al. Oestrogen receptor-regulated glutathione S-transferase mu 3 expression attenuates hydrogen peroxide-induced cytotoxicity, which confers tamoxifen resistance on breast cancer cells. Breast Cancer Res Treat. 2018;172(1):45-59.
56. Gasch AP, Huang M, Metzner S, Botstein D, Elledge SJ, Brown PO. Genomic expression responses to DNA-damaging agents and the regulatory role of the yeast ATR homolog Mec1p. Mol Biol Cell. 2001;12(10):2987-3003.
57. Alvaro D, Lisby M, Rothstein R. Genome-wide analysis of Rad52 foci reveals diverse mechanisms impacting recombination. PLoS Genet. 2007;3(12):e228.
58. Perry JJ, Ballard GD, Albert AE, Dobrolecki LE, Malkas LH, Hoelz DJ. Human C6orf211 encodes Armt1, a protein carboxyl methyltransferase that targets PCNA and is linked to the DNA damage response. Cell Rep. 2015;10(8):1288-96.
59. Deutsch EW, Bandeira N, Perez-Riverol Y, Sharma V, Carver JJ, Mendoza L, et al. The ProteomeXchange consortium at 10 years: 2023 update. Nucleic Acids Res. 2023;51(D1):D1539-d48.
60. Perez-Riverol Y, Bai J, Bandla C, García-Seisdedos D, Hewapathirana S, Kamatchinathan S, et al. The PRIDE database resources in 2022: a hub for mass spectrometry-based proteomics evidences. Nucleic Acids Res. 2022;50(D1):D543-d52.
61. Michaelis M, Rothweiler F, Barth S, Cinatl J, van Rikxoort M, Löschmann N, et al. Adaptation of cancer cells from different entities to the MDM2 inhibitor nutlin-3 results in the emergence of p53-mutated multi-drug-resistant cancer cells. Cell Death Dis. 2011;2(12):e243.

62. Gagliano T, Shah K, Gargani S, Lao L, Alsaleem M, Chen J, et al. PIK3Cδ expression by fibroblasts promotes triple-negative breast cancer progression. J Clin Invest. 2020;130(6):3188-204.
63. Franken NA, Rodermond HM, Stap J, Haveman J, van Bree C. Clonogenic assay of cells in vitro. Nat Protoc. 2006;1(5):2315-9.
64. Gundogdu R, Erdogan MK, Ditsiou A, Spanswick V, Garcia-Gomez JJ, Hartley JA, et al. hMOB2 deficiency impairs homologous recombination-mediated DNA repair and sensitises cancer cells to PARP inhibitors. Cell Signal. 2021;87:110106.
65. Ditsiou A, Cilibrasi C, Simigdala N, Papakyriakou A, Milton-Harris L, Vella V, et al. The structure-function relationship of oncogenic LMTK3. Sci Adv. 2020;6(46).
66. Agnarelli A, Lauer Betrán A, Papakyriakou A, Vella V, Samuels M, Papanastasopoulos P, et al. The Inhibitory Properties of a Novel, Selective LMTK3 Kinase Inhibitor. Int J Mol Sci. 2023;24(1).
67. Stebbing J, Shah K, Lit LC, Gagliano T, Ditsiou A, Wang T, et al. LMTK3 confers chemo-resistance in breast cancer. Oncogene. 2018;37(23):3113-30.
68. Cilibrasi C, Ditsiou A, Papakyriakou A, Mavridis G, Eravci M, Stebbing J, et al. LMTK3 inhibition affects microtubule stability. Mol Cancer. 2021;20(1):53.
69. Coughlan AM, Harmon C, Whelan S, O'Brien EC, O'Reilly VP, Crotty P, et al. Myeloid Engraftment in Humanized Mice: Impact of Granulocyte-Colony Stimulating Factor Treatment and Transgenic Mouse Strain. Stem Cells Dev. 2016;25(7):530-41.
70. Shultz LD, Lyons BL, Burzenski LM, Gott B, Chen X, Chaleff S, et al. Human lymphoid and myeloid cell development in NOD/LtSz-scid IL2R gamma null mice engrafted with mobilized human hemopoietic stem cells. J Immunol. 2005;174(10):6477-89.
71. Valenti F, Sacconi A, Ganci F, Grasso G, Strano S, Blandino G, et al. The miR-205-5p/BRCA1/RAD17 Axis Promotes Genomic Instability in Head and Neck Squamous Cell Carcinomas. Cancers (Basel). 2019;11(9).
72. Kim CJ, Terado T, Tambe Y, Mukaisho KI, Sugihara H, Kawauchi A, et al. Anti-oncogenic activities of cyclin D1b siRNA on human bladder cancer cells via induction of apoptosis and suppression of cancer cell stemness and invasiveness. Int J Oncol. 2018;52(1):231-40.
73. Rampias T, Karagiannis D, Avgeris M, Polyzos A, Kokkalis A, Kanaki Z, et al. The lysine-specific methyltransferase KMT2C/MLL3 regulates DNA repair components in cancer. EMBO Rep. 2019;20(3).
74. Giamas G, Filipović A, Jacob J, Messier W, Zhang H, Yang D, et al. Kinome screening for regulators of the estrogen receptor identifies LMTK3 as a new therapeutic target in breast cancer. Nat Med. 2011;17(6):715-9.
75. Stebbing J, Filipovic A, Ellis IO, Green AR, D'Silva TR, Lenz HJ, et al. LMTK3 expression in breast cancer: association with tumor phenotype and clinical outcome. Breast Cancer Res Treat. 2012;132(2):537-44.
76. Wiśniewski JR, Zougman A, Nagaraj N, Mann M. Universal sample preparation method for proteome analysis. Nat Methods. 2009;6(5):359-62.

77. Gilar M, Olivova P, Daly AE, Gebler JC. Two-dimensional separation of peptides using RP-RP-HPLC system with different pH in first and second separation dimensions. J Sep Sci. 2005;28(14):1694-703.
78. Olsen JV, de Godoy LM, Li G, Macek B, Mortensen P, Pesch R, et al. Parts per million mass accuracy on an Orbitrap mass spectrometer via lock mass injection into a C-trap. Mol Cell Proteomics. 2005;4(12):2010-21.
79. Cox J, Neuhauser N, Michalski A, Scheltema RA, Olsen JV, Mann M. Andromeda: a peptide search engine integrated into the MaxQuant environment. J Proteome Res. 2011;10(4):1794-805.
80. Yu G, Wang LG, Han Y, He QY. clusterProfiler: an R package for comparing biological themes among gene clusters. Omics. 2012;16(5):284-7.
81. ten Cate B, Samplonius DF, Bijma T, de Leij LF, Helfrich W, Bremer E. The histone deacetylase inhibitor valproic acid potently augments gemtuzumab ozogamicin-induced apoptosis in acute myeloid leukemic cells. Leukemia. 2007;21(2):248-52.

Figures

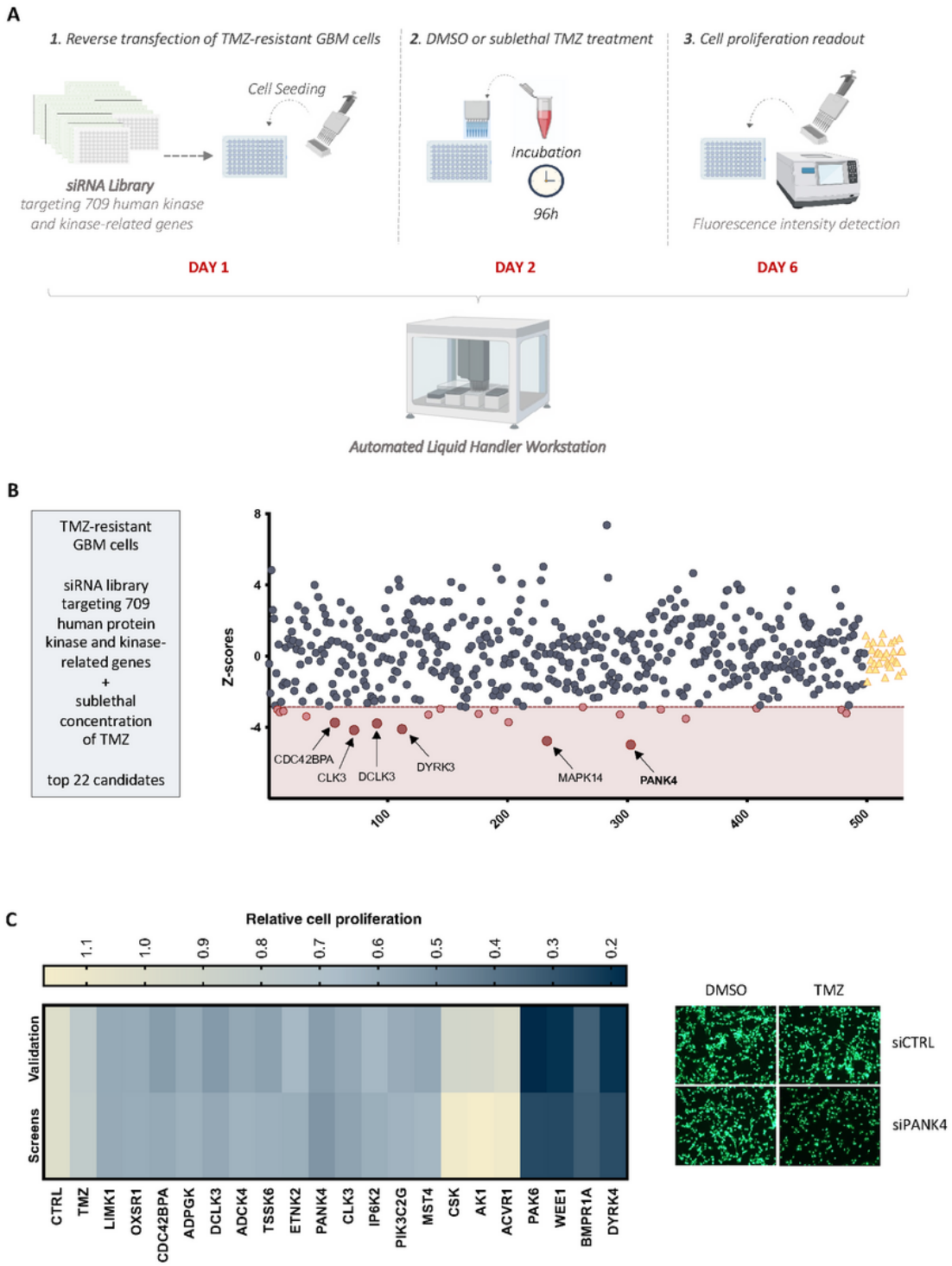

Figure 1

Kinome-wide RNAi screen identifies PANK4 as a synthetic lethal partner of TMZ. (**A**) Schematic representation of the synthetic lethal RNAi screen workflow. U87MG^{Res} cells were reverse-transfected using an siRNA library targeting 709 human protein kinase and kinase-related genes. 24 hours after transfection, cells were treated with either DMSO or a sublethal concentration of TMZ and incubated for 96 hours. On day 6, CyQuant reagent was added to the cells and fluorescence intensity was quantified as

a measure of cell proliferation. Figure was created with BioRender.com. (**B**) Z-scores of synthetic lethal candidate genes generated from the RNAi primary screens. Red dots represent top-candidates that significantly decreased cell proliferation in combination with TMZ (z-score cut-off: <−2.86). Yellow triangles represent TMZ controls. (**C**) *Left:* Smaller-scale secondary screen on U87MG^{Res} cells compared to our primary screens (average of two independent screens). The heatmap displays the combined effect of gene knockdown and TMZ treatment on cell proliferation calculated for each of the indicated kinases. Blue and yellow denote either reduction or increase in cell proliferation, respectively. *Right:* Representative images of U87MG^{Res} cells labelled with CyQuant green fluorescent nucleic acid stain, demonstrating the antiproliferative effect of PANK4 knockdown and sublethal TMZ treatment. Magnification, 10X.

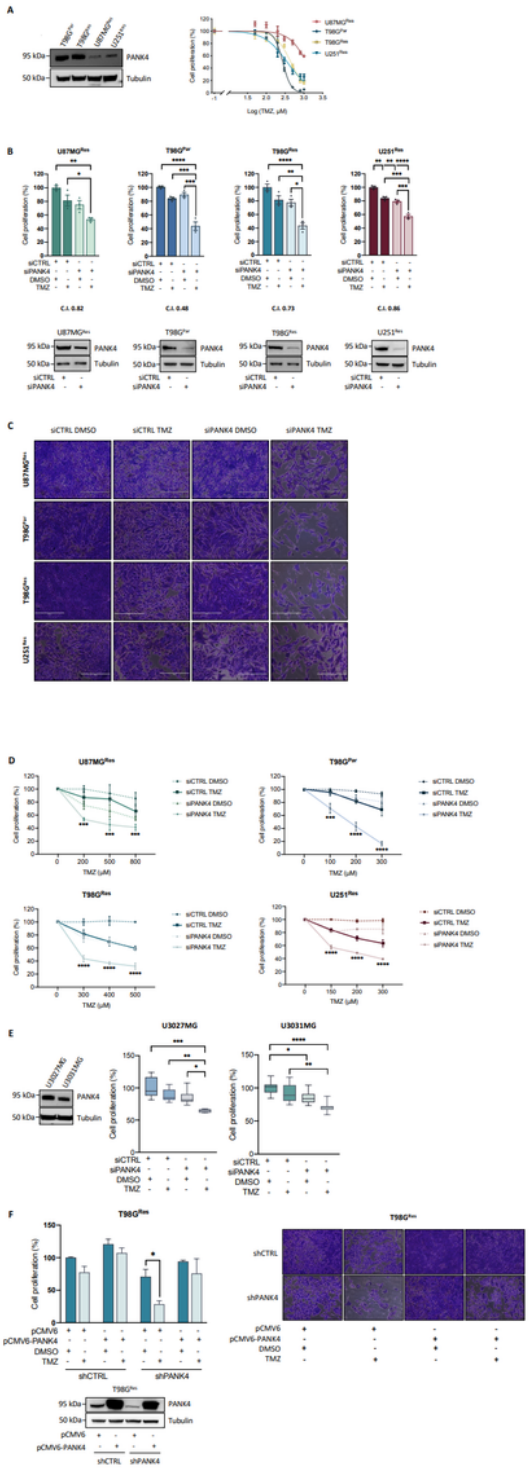

Figure 2

PANK4 knockdown enhances the chemosensitivity of TMZ-resistant GBM cells. (**A**) *Left:* Western blot showing PANK4 protein expression levels in the indicated TMZ-resistant GBM cell lines. Tubulin was used as loading control. *Right:* The same cancer cell lines were treated with increasing concentrations of TMZ and their dose response curves are shown. Cell proliferation was assessed at 96 hours and sublethal concentrations of TMZ were determined for all cell lines, following calculation of IC_{20} values using the

GraphPad Prism 9 software. (**B**) Cells were transfected with either siCTRL or siPANK4 and treated with sublethal concentrations of TMZ or DMSO after 24 hours. Cell proliferation was evaluated at 96 hours. The Cooperativity Index (CI) is shown for each cell line. PANK4 knockdown was confirmed by western blotting. Tubulin was used as loading control. (**C**) Representative images of the proliferation assays shown in **B**. Magnification, 10X. Scale bar, 400 mm. (**D**) Cells were transfected with either siCTRL or siPANK4 for 24 hours and treated with increasing concentrations of TMZ or DMSO, as indicated. Cell proliferation was assessed after 96 hours. (**E**) *Left:* Western blot showing PANK4 protein expression levels in the indicated patient-derived GBM cell lines. Tubulin was used as loading control. *Right:* Cell proliferation of the same cells, following transfection with either siCTRL or siPANK4 and treatment with sublethal concentrations of TMZ or DMSO, as described in **B**. (**F**) Control and stably PANK4-depleted T98G^{Res} cells (shCTRL/shPANK4) were transfected with either pCMV6 or PCMV6-PANK4. After 24 hours, cells were treated with DMSO or TMZ. The effect of PANK4 overexpression on cell proliferation was assessed after 96 hours. Representative images and western blot analysis of PANK4 protein expression are shown. Tubulin was used as loading control. All data are presented as mean ± SEM. Each experiment was conducted at least three times. Statistical analysis was performed using two-way ANOVA (**B**, **D**, **E**, **F**); asterisks (*) designate significant differences between conditions indicated with brackets (**B**, **E**, **F**) or compared with the corresponding DMSO-treated siRNA controls (**D**) (*p*-values: *$p < 0.05$, **$p < 0.01$, ***$p < 0.001$, and ****$p < 0.0001$).

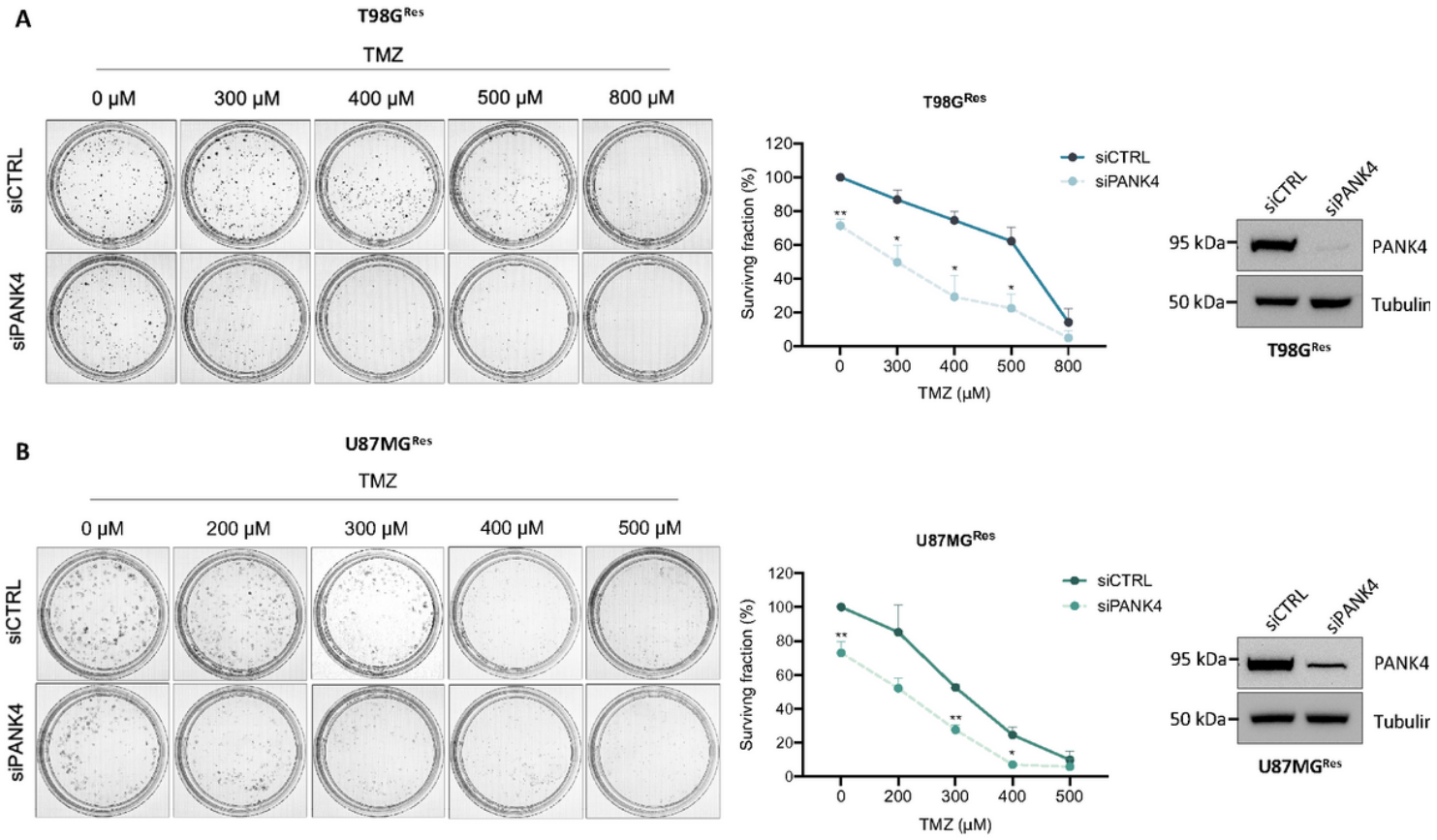

Figure 3

PANK4 depletion potentiates TMZ cytotoxicity by reducing the clonogenic potential of resistant GBM cell lines. (**A**) Representative images of colony formation assays in control or PANK4-depleted T98G^{Res} and (**B**) U87MG^{Res} cells following treatment with TMZ, as indicated. Colonies were quantified and results show the percentage of colonies formed after treatment with the indicated concentrations of the drug (surviving fraction), corrected according to the plating efficiencies of the corresponding controls. PANK4 silencing was confirmed by western blot. Tubulin was used as loading control. Data are shown as mean ± SEM (n = 3 biological replicates). Significance was determined using unpaired Student's t-test; asterisks (*) designate significant differences compared with the corresponding TMZ-treated siRNA controls (*p*-values: *$p < 0.05$, **$p < 0.01$).

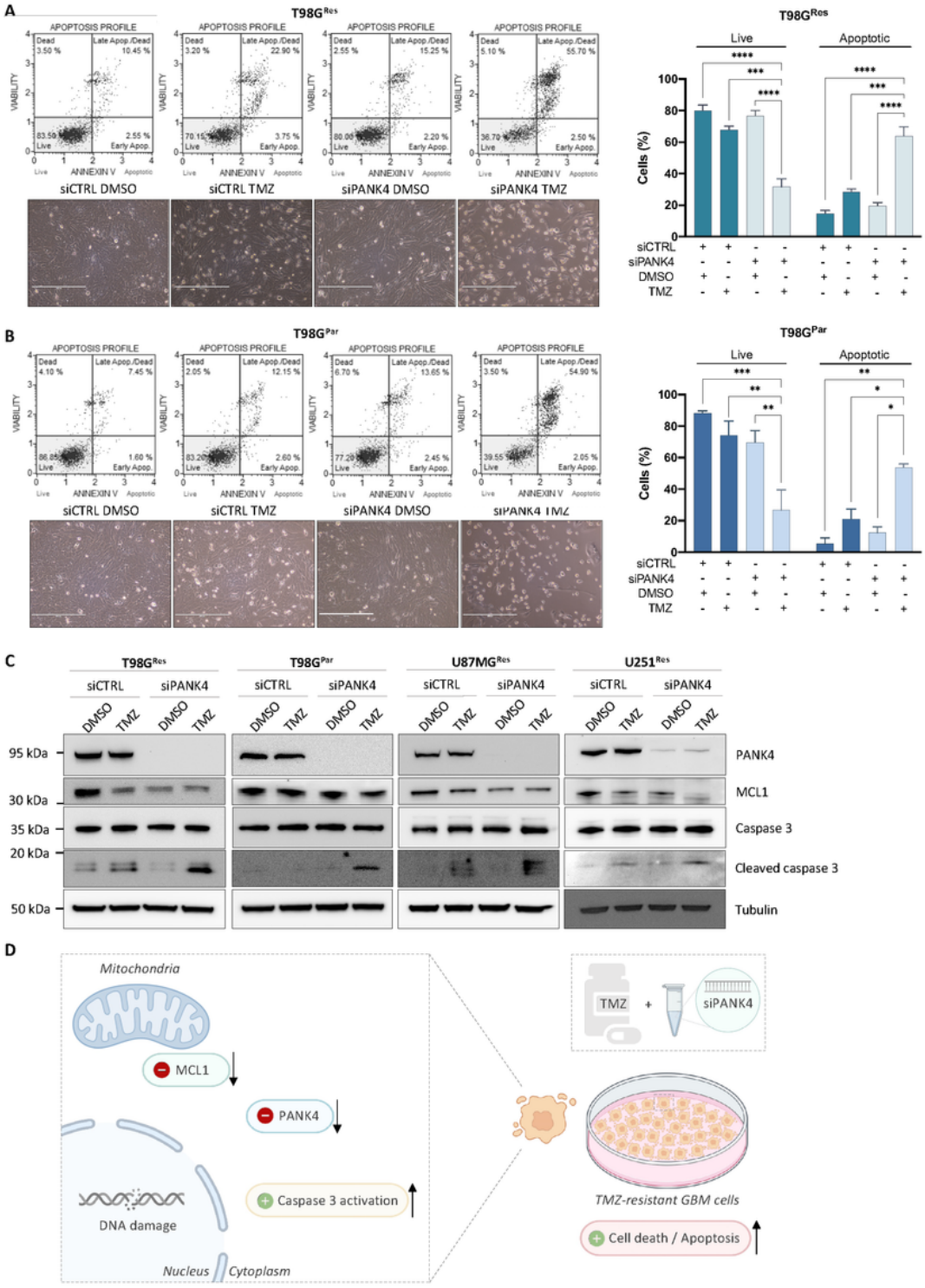

Figure 4

Figure 4

PANK4 downregulation induces apoptotic cell death upon TMZ treatment. (**A**) T98G^{Res} and (**B**) T98G^{Par} cells were transfected with either siCTRL or siPANK4. 24 hours after transfection, treatments with sublethal concentrations of TMZ were performed and the percentages of apoptotic cells were determined following annexin V and 7-AAD staining (96 hours). Representative plots are shown. All data are presented as mean ± SEM. Each experiment was conducted at least three times. Statistical analysis was

performed using two-way ANOVA; asterisks (*) designate significant differences between conditions indicated with brackets (*p*-values: *$p < 0.05$, **$p < 0.01$, ***$p < 0.001$, and ****$p < 0.0001$). (**C**) Western blots showing expression of PANK4, MCL1, caspase 3 and cleaved caspase 3 in control and PANK4-depleted T98G^{Res}, T98G^{Par}, U87MG^{Res} and U251^{Res} cells treated with DMSO or TMZ for 96 hours. Tubulin was used as loading control. (**D**) Schematic representation of apoptotic cell death following combined PANK4 silencing and TMZ treatment. Figure was created with BioRender.com.

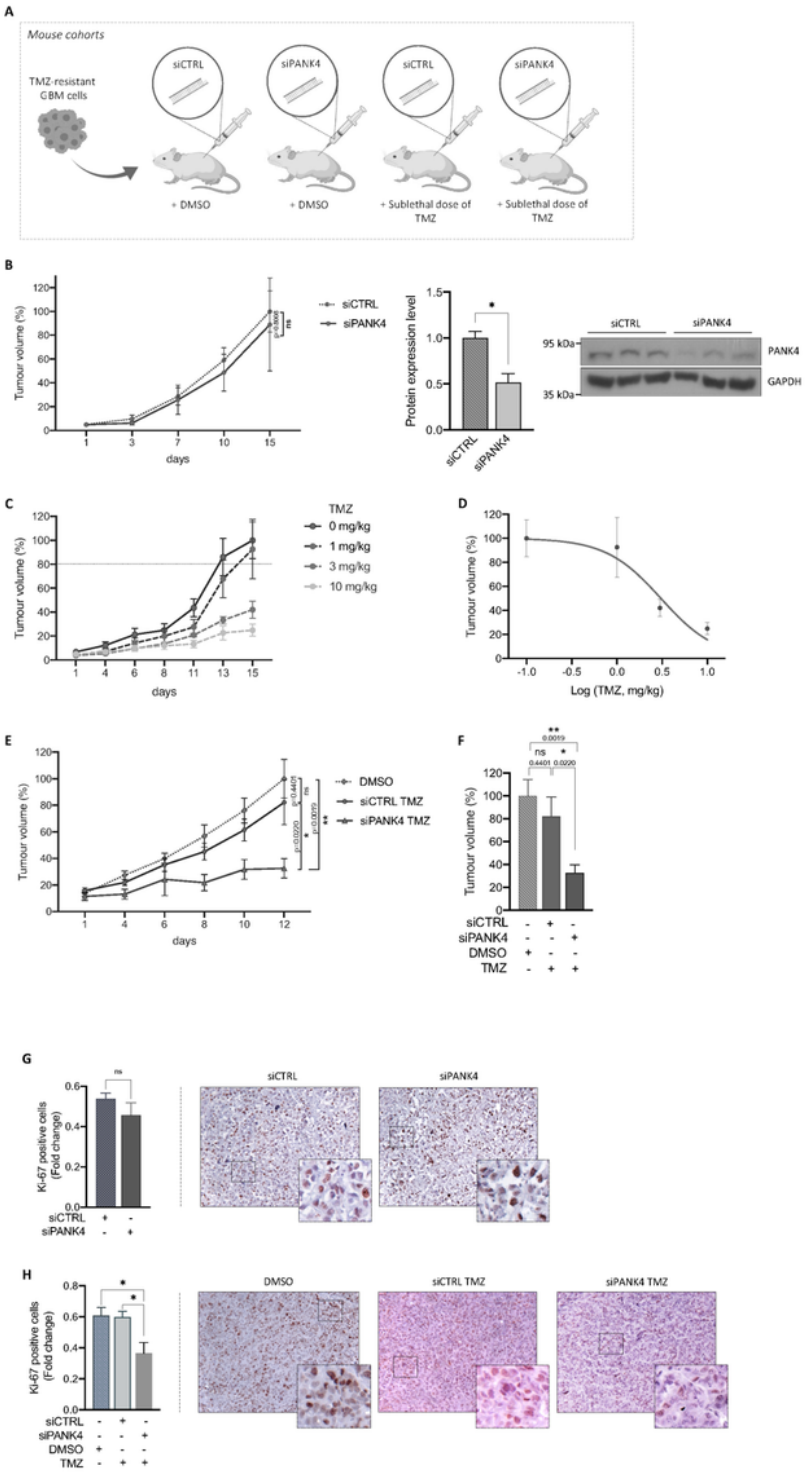

Figure 5

Abrogation of PANK4 sensitises chemoresistant GBM tumours to TMZ treatment *in vivo*. (**A**) Schematic representation of the experimental design of our *in vivo* study. Four mouse cohorts were established: siCTRL DMSO, siPANK4 DMSO, siCTRL TMZ and siPANK4 TMZ (n=6 mice per group). Figure was created with BioRender.com. (**B**) Effect of PANK4 knockdown on tumour growth of mice carrying $T98G^{Res}$ xenografts (n=6 mice per group). Western blot and densitometric analysis of PANK4 expression in tumour lysates from three distinct tumours is shown confirming PANK4 knockdown efficiency. GAPDH was used as loading control. Error bars represent ± SEM. Significance was calculated using unpaired Student's t-test; asterisks (*) designate significant differences between conditions indicated with brackets (ns, not significant; *$p < 0.05$). (**C**) $T98G^{Res}$ xenograft mice were treated with either vehicle control or TMZ at the indicated concentrations (n=6 mice per group) and (**D**) the *in vivo* sublethal dose of TMZ was subsequently determined using the GraphPad Prism 9 software. (**E** and **F**) Effect of combined PANK4 knockdown and treatment with the sublethal dose of TMZ on tumour growth of $T98G^{Res}$ xenograft mice. (**G**) Immunohistochemical (IHC) evaluation of Ki-67 expression in tumour sections from $T98G^{Res}$ xenograft mice following PANK4 knockdown or (**H**) treated with the sublethal dose of TMZ alone or following PANK4 depletion. Fold change of Ki-67-positive cells versus the total number of cells is shown. Data represent average of four independent samples per cohort, in duplicate. Representative images of Ki-67 immunohistochemical staining in harvested tumours from each cohort are presented. Original magnification, x20. Scale bar, 50 mm. (**E**-**H**) Results are expressed as mean ± SEM. Significance was calculated using unpaired Student's t-test; asterisks (*) designate significant differences between conditions indicated with brackets (ns, not significant; *$p < 0.05$, **$p < 0.01$).

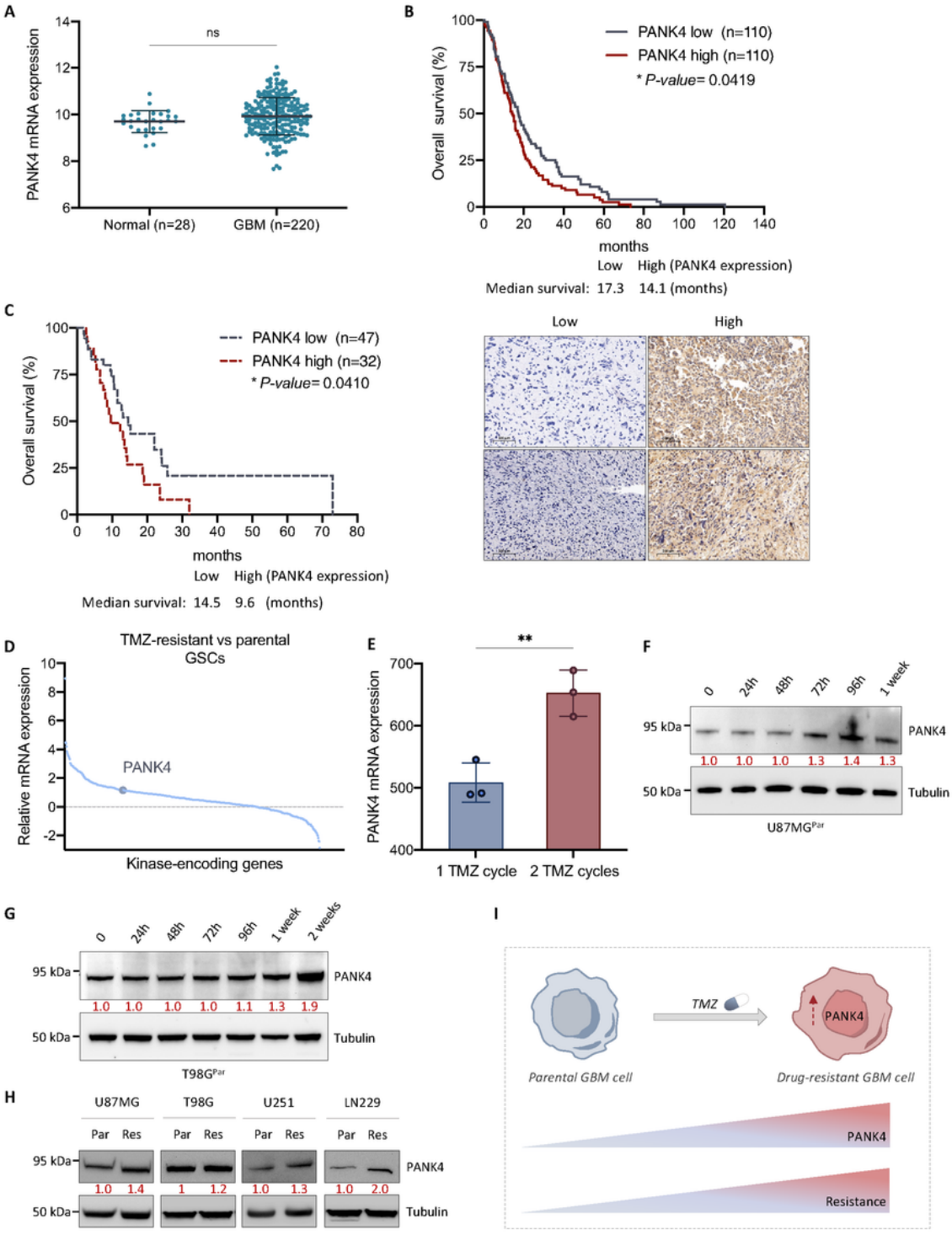

Figure 6

Figure 6

PANK4 expression profile in GBM patient cohorts and its association with TMZ resistance. (**A**) Relative PANK4 mRNA expression in normal versus GBM tissue samples. Data derived from the Rembrandt brain cancer dataset (https://gdoc.georgetown.edu) (26). (**B**) Kaplan-Meier survival analysis showing the association between PANK4 mRNA expression and overall survival (OS) of GBM patients within the Rembrandt database and (**C**) Kaplan-Meier plot showing the association between PANK4 protein

expression, assessed by immunohistochemical analysis (IHC), and OS of GBM IDH-wildtype patients. Statistical significance was evaluated by log-rank analysis. Representative images of low and high immunohistochemical staining intensity of PANK4 protein expression in GBM tissue sections are shown alongside. Scale bar, 100 mm. (**D**) Analysis for differentially expressed kinases (DEKs) in TMZ-resistant versus parental GBM stem cells (GSCs). PANK4 was upregulated in the TMZ-resistant group. Figure was generated based on data from the Gene Expression Omnibus (GEO; www.ncbi.nlm.nih.gov/geo, accession number: GSE68029) (28, 29). (**E**) Analysis of PANK4 mRNA expression in TMZ-resistant GSCs that survived either one or two cycles of TMZ. Data from the GEO (www.ncbi.nlm.nih.gov/geo, accession number: GSE68029) (28). (**F**) Representative western blots of PANK4 protein expression in $U87MG^{Par}$ and (**G**) $T98G^{Par}$ cells, following treatment with the TMZ concentrations used to generate their resistant counterparts, for the indicated time points. Tubulin was used as loading control. (**H**) Representative western blots of the protein expression levels of PANK4 in parental versus TMZ-resistant cell lines (U87MG, T98G, U251, LN229). Tubulin was used as loading control. (**F**-**H**) Densitometric analysis of PANK4 expression is shown. (**I**) Schematic model illustrating the involvement of PANK4 in TMZ resistance in GBM. Figure was created with BioRender.com. (**A**, **E**) Error bars represent SD. Significance

was determined by unpaired Student's t-test (ns, not significant; $^{**}p < 0.01$).

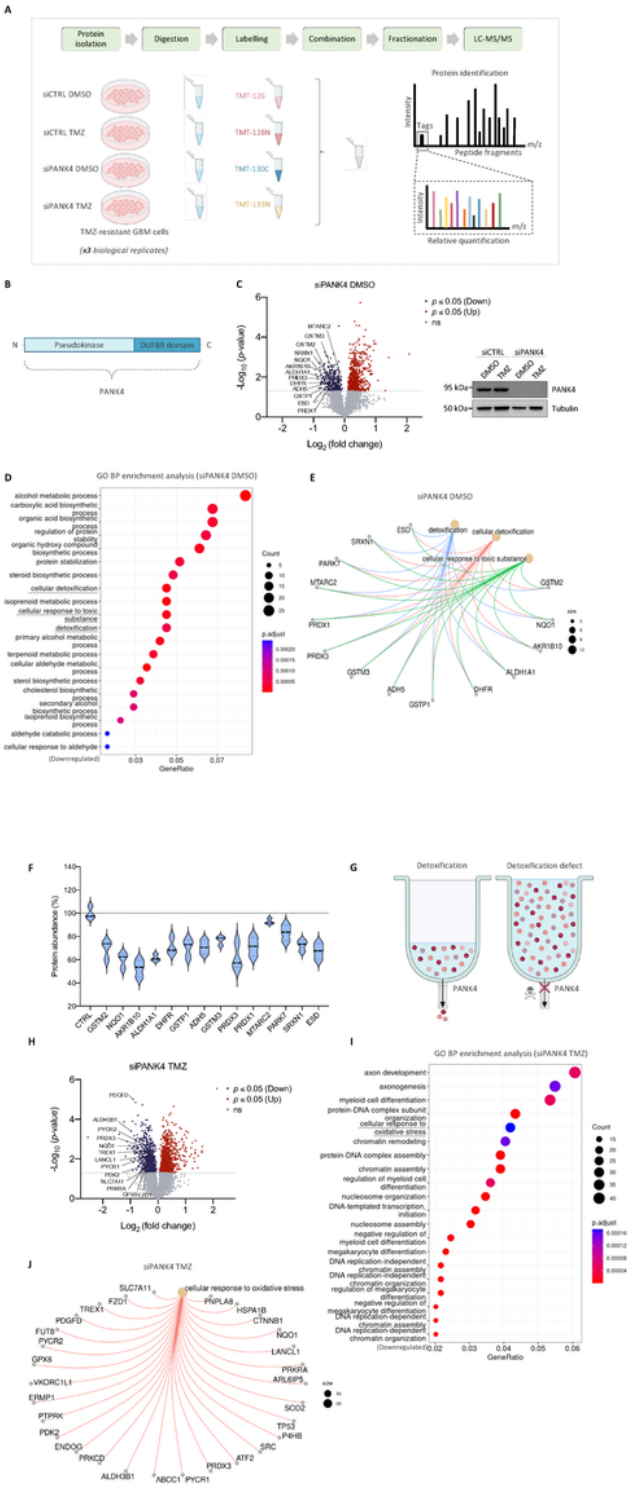

Figure 7

TMT-based proteomic analysis reveals reduced cell detoxification response upon PANK4 knockdown. (**A**) Schematic representation of the Tandem Mass Tag (TMT) proteomic experiment. The following four conditions were assessed in T98G^{Res} cells: siCTRL DMSO, siCTRL TMZ, siPANK4 DMSO and siPANK4 TMZ (n=3 biological replicates). Figure was created with BioRender.com. (**B**) Schematic diagram showing the PANK4 protein domains. Adapted from Huang *et al.* (2016) (17). (**C**) Volcano plot of differentially

expressed proteins following PANK4 knockdown in T98G^{Res} cells (siPANK4 DMSO), highlighting statistically significant changes ($p \leq 0.05$) in protein abundance compared to control (siCTRL DMSO). The -Log_{10}(*p*-values) vs the Log_2(fold change) in protein abundance are plotted. Horizontal line represents the significant threshold ($p = 0.05$). Red and blue circles indicate significantly up- or down-regulated proteins, respectively. Grey circles indicate proteins with non-significant changes in abundance following PANK4 silencing; (ns, not significant). Validation of PANK4 protein levels by western blot using tubulin as loading control is shown. (**D**) Dotplot showing the top 20 significantly enriched Gene Ontology (GO) Biological Processes (BP) of downregulated proteins following PANK4 knockdown (siPANK4 DMSO vs siCTRL DMSO). (**E**) Cnetplot depicting the 14 significantly downregulated proteins involved in the GO BP terms of interest, including “cellular detoxification”, “cellular response to toxic substance” and “detoxification”. (**F**) Violin plot showing abundance of the proteins highlighted in (**E**). (**G**) Schematic model of PANK4 involvement in cellular detoxification of TMZ-resistant GBM cells. Adapted from Lee *et al.* (2020) (39). Figure was created with BioRender.com. (**H**) Volcano plot of differentially expressed proteins following combined PANK4 knockdown and TMZ treatment of T98G^{Res} cells was generated (siPANK4 TMZ) as in (**C**); statistically significant changes in protein abundance ($p \leq 0.05$) compared to control (siCTRL DMSO) are shown. (**I**) Dotplot displaying the top 20 significantly enriched GO BP terms of downregulated proteins following combined silencing of PANK4 and treatment with TMZ (siPANK4 TMZ vs siCTRL DMSO). (**J**) Cnetplot depicting the 29 significantly downregulated proteins associated with the GO BP term “cellular response to oxidative stress”.

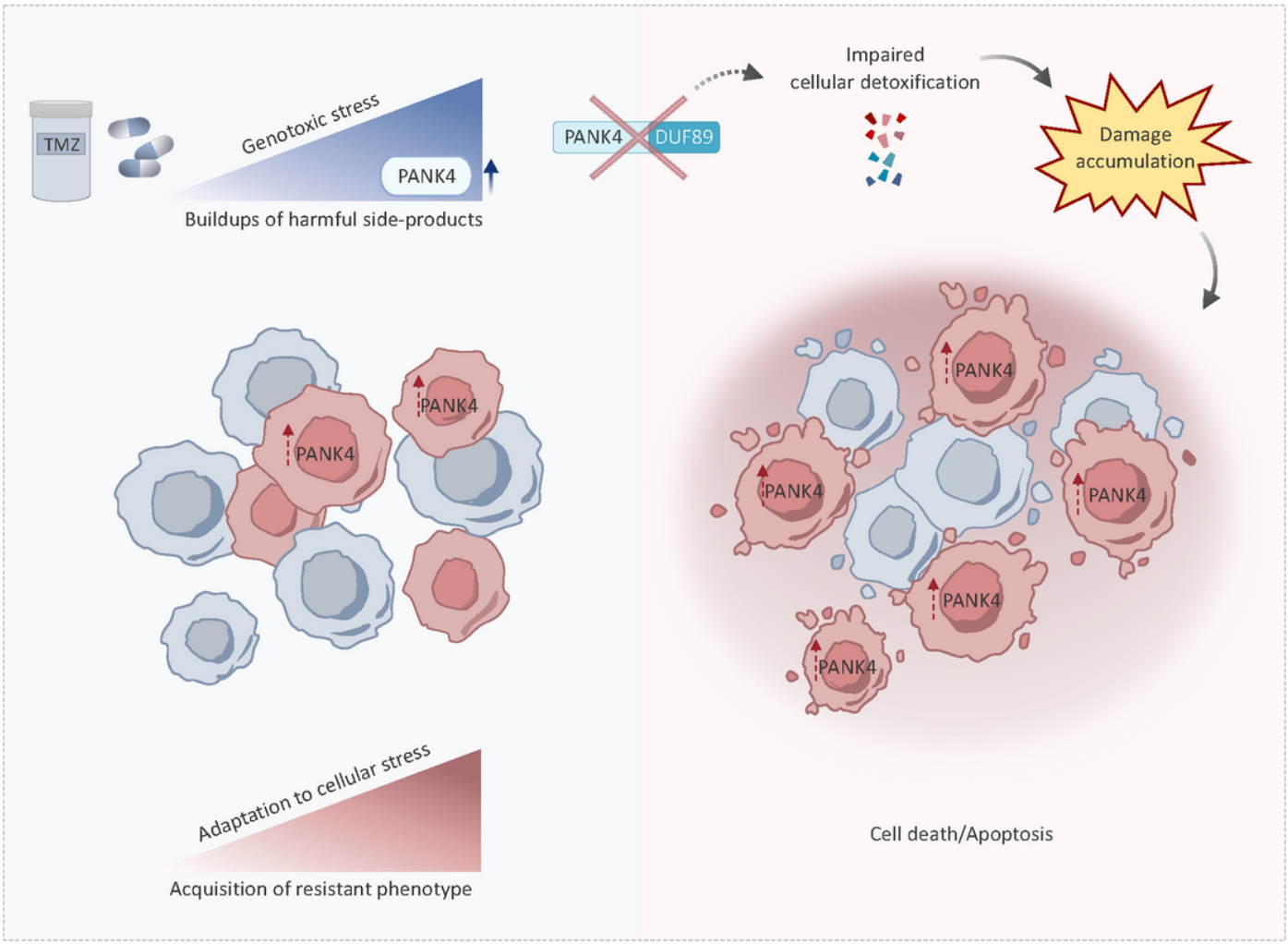

Figure 8

Schematic model depicting the role of PANK4 in TMZ resistance in GBM.

Supplementary Files

This is a list of supplementary files associated with this preprint. Click to download.

- SupplementaryFigures.pdf
- SupplementaryTables.xlsx
- Figure0GraphicalAbstract.pdf